Boundary Value Problems
a SpringerOpen Journal

RESEARCH Open Access

Robust and accurate numerical framework for multi-dimensional fractional-order telegraph equations using Jacobi/Jacobi-Romanovski spectral technique

M.A. Abdelkawy[1,2], Mohammad Izadi[3*] and Waleed Adel[4,5]

*Correspondence: izadi@uk.ac.ir
[3]Department of Applied Mathematics, Faculty of Mathematics and Computer, Shahid Bahonar University of Kerman, Kerman, Iran
Full list of author information is available at the end of the article

Abstract

This paper presents a novel spectral algorithm for the numerical solution of multi-dimensional fractional-order telegraph equations, a critical model used to capture the combined effects of diffusion and wave propagation. The core innovation of this work is the application of Jacobi-Romanovski polynomials as the basis functions for spectral discretization. These polynomials offer unique advantages, including the ability to handle nonstandard domains and boundary conditions, making them particularly suitable for partial differential equation (PDE) applications. A comprehensive error analysis is conducted, providing deep insights into the convergence rates and factors affecting the accuracy of the numerical solutions. Extensive numerical experiments further demonstrate the superior performance of the proposed spectral algorithm in solving a wide range of multi-dimensional fractional-order telegraph equation models. The results show a significant improvement in accuracy and computational efficiency compared to traditional numerical methods, such as finite difference or finite element techniques. This research advances the field of computational science by offering a robust, efficient, and versatile numerical framework for the precise solution of complex multi-dimensional PDEs.

Mathematics Subject Classification: 65L60; 41A10; 35R11; 65M15

Keywords: Liouville-Caputo fractional derivative; Jacobi polynomials; Collocation points; Romanovski-Jacobi functions; Error bound; Fractional telegraph differential equations

1 Introduction

Over the past few years, fractional calculus (FC) has emerged as a rapidly expanding field of science that has gained significant attention, with diverse applications ranging from physics, engineering, natural phenomena, and even financial modeling [1]. In many physical systems, particularly those involving diffusion and wave propagation, the behavior of the system is influenced not only by its current state but also by its historical evolution.

This memory effect is naturally captured through the use of fractional-order derivatives. Unlike classical integer-order derivatives, which describe the rate of change of a quantity at a given moment, fractional derivatives incorporate an integral term that accounts for all prior states of the system. In the context of the fractional-order telegraph equations considered in this study, the fractional derivative allows for more nuanced modeling of processes with memory and hereditary properties, making it especially relevant in multi-dimensional scenarios. This ensures that the model accounts for both local dynamics and cumulative effects from the past, providing a more accurate representation of real-world phenomena. Several fractional definitions have been used across various disciplines, such as viscoelasticity, biology, electrical engineering, and others [2]. These fractional definitions have proven particularly valuable in the formulation of differential equations for simulating complex problems or phenomena, often involving memory-related or delayed effects. Although many physical processes can be adequately described only in terms of their current state, many other processes are better modeled by considering the dependence on the previous states [3]. In such cases, incorporating historical information into the model can lead to more accurate representations, albeit with increased complexity. These definitions may include Riemann-Liouville [4], Caputo [5], Caputo-Fabrizio [6], and Atangana-Baleanu derivatives [7]. Each of these operators has its advantages and disadvantages. Among others, one of the most widely and important used operators is the Caputo or, more precisely, Liouville-Caputo fractional definition. The Caputo fractional derivative is a powerful mathematical tool that has found widespread applications in various fields. One of the primary benefits of the Caputo fractional derivative, compared to other fractional definitions, is its compatibility with the traditional initial conditions used in the study of differential equations. Unlike the Riemann-Liouville fractional derivative operator, which requires the specification of fractional-order initial conditions, the Caputo formulation allows for more intuitive and familiar initial conditions. This property facilitates the integration of the Caputo fractional derivative into existing mathematical frameworks and simplifies the interpretation of the resulting models. Another important advantage is its improved numerical stability, particularly when dealing with noisy or irregular data. The Caputo definition tends to be more robust to these challenges compared to other fractional derivative definitions, which can be more susceptible to numerical instabilities. This enhanced numerical stability is crucial in the analysis of real-world systems, where noise and uncertainties are often presented. With these important remarks, the Caputo definitions have been used in the simulations of models with physical importance. For example, the Caputo fractional derivative has been used for simulating and understanding the dynamics of the Nipah virus by Evirgen [8]. In addition, Bhangale et al. [9] utilized the definition of the Caputo derivative for simulating the Maxwell model arising in the simulation of fluid dynamics. A hybrid kernel functions-based collocation strategy has also been adopted by Li et al. [10] for solving boundary value problems. These are only some models that have recently used the definition of the Caputo derivative. For more information, the reader may refer to [11–14] and the references therein.

One of the most important topics is communication networks, which are related to the exchange of information between different locations. This transmission is done through a medium known as the transmission medium, which can be categorized into guided and unguided mediums. The guided transmission media can be described by the signal contained within a conductive channel or medium. An example of such a medium is the cable

transmission media, which provides a physical infrastructure for the widespread distribution of messages between multiple locations [15, 16]. To better understand the transmission of a such signal, mathematical modeling can be utilized to simulate this signal. This model can be expressed by a second-order hyperbolic Partial Differential Equation (PDE) known as a telegraph equation. The properties of the telegraph equation are commonly utilized to model the propagation of electrical currents through cables, with applications in various fields such as neutron transport, random walk analysis, signal processing, electrical signal transmission, molecular dynamics, and others. The one-dimensional telegraph equation can represent wave propagation without leakage or resistance, as well as diffusion processes without significant leakage or inductance [17, 18]. In recent years, the telegraph equation has been recognized as a more suitable model compared to the traditional diffusion equation for studying reaction-diffusion dynamics in various scientific and technological domains.

Spectral and collocation methods have emerged as powerful tools for solving complex differential equations, particularly those involving fractional derivatives and multi-dimensional domains. Spectral methods, which utilize basis functions such as orthogonal polynomials or wavelets, are renowned for their accuracy and efficiency in capturing the nuances of fractional-order dynamics. For instance, wavelet-based computational algorithms have been successfully applied to multi-dimensional distributed-order fractional differential equations with nonlinear source terms, demonstrating the capability of wavelets to manage complex boundary and source term interactions [19]. Similarly, wavelet approaches have been adapted for financial mathematical models governed by distributed-order fractional differential equations, showcasing their versatility in various applications [20]. Collocation methods, on the other hand, involve approximating the solution at discrete points, leveraging basis functions to solve the differential equations efficiently. Noteworthy advancements include the development of a collocation method for time-fractional diffusion equations on metric star graphs, which has provided significant insights into the behavior of fractional systems [21], see also [22]. Additionally, wavelet collocation methods based on Gegenbauer scaling functions have been employed to solve fourth-order time-fractional integro-differential equations with weakly singular kernels, illustrating their effectiveness in handling singularities [23]. The use of Legendre wavelets in collocation methods for coupled time-fractional nonlinear diffusion systems further highlights the strength of wavelet-based techniques in both linear and nonlinear scenarios [24]. Moreover, recent work on numerical techniques based on Legendre wavelets for hyperbolic telegraph equations underscores their applicability to complex telegraph models [25]. Finally, the integration of wavelet-based approximations with nonstandard finite difference schemes has been explored for singularly perturbed partial integro differential equations, providing a robust framework for addressing challenging computational problems [26, 27].

Currently, researchers are paying considerable attention to the advancement, investigation, and development of appropriate techniques for solving fractional-order telegraph equation (FOTE). Various scholars have gained the analytical results of the FOTE using different techniques, including Laplace transforms, Fourier transforms, and transform inversion as some examples of the techniques used [28]. The analytical solution of the space-time FOTE has been obtained by applying the double Laplace transform method [29]. Similarly, the double Laplace transform method has been utilized to derive analytical solutions

of the time-fractional wave equation under non-homogeneous Neumann and Dirichlet boundary conditions [30]. On the other side, researchers have proposed several methods for solving the second-order hyperbolic telegraph equation in 1D. Mittal et al. [31] suggested an approach based on the definition of the cubic B-spline collocation for solving the FOTE. In addition, Nazir et al. [32] adapted the new cubic trigonometric B-splines for solving the second-order hyperbolic telegraph equation. Another technique is the meshless approach based on collocation methodology, which uses the radial bases in space and the orthogonal Chebyshev polynomials in time and has been employed by Bansu et al. [33]. Additionally, the Bernstein polynomial operational matrices method has been applied to find solutions of the fractional-order telegraph equation [34]. Marasi et al. [35] also developed a method based on the fractional-order Gegenbauer wavelet technique for solving the multi-term FOTE with distributed order. Other methods that have been used for solving the model can be found in [36–38] and references therein.

In this manuscript, we are mainly interested in adapting a novel collocation approach for solving the multi-dimensional fractional-order telegraph equation using the classical Jacobi and (novel) Jacobi-Romanovski polynomials as basis functions. The Jacobi polynomials are used for approximating the space variable while opting for Romanovski-Jacobi polynomials to approximate the time variable. Although Jacobi polynomials could theoretically be used for both directions, Romanovski-Jacobi polynomials provide distinct advantages when dealing with time-dependent fractional-order models. These polynomials are orthogonal polynomials that play a significant role in mathematical analysis as well as in approximation theory. In addition, these polynomials are particularly well-suited for functions with asymptotic behavior or when the solution involves wave-like structures. Their orthogonality in the unbounded domain and their ability to better capture oscillatory and decaying behavior make them an ideal choice for approximating time dynamics in telegraph equations. By using Romanovski-Jacobi polynomials, we enhance the accuracy and robustness of the solution when modeling time-dependent processes in multi-dimensional spaces, especially in the presence of fractional orders, where memory and hereditary properties are significant. Numerous successful applications of spectral orthogonal methodologies can be tracked in the previously accomplished works [39–44]. The importance of studying the multi-dimensional fractional-order FOTE lies in its potential for better understanding the possible applications of such models. To the best of the authors' knowledge, this is the first time the fractional multi-term FOTE model has been studied using the fractional Jacobi-Romanovski collocation approach. The novelty of this paper lies in the following points:

1. A novel development of a spectral algorithm for the numerical study of multi-dimensional telegraph equations of fractional order.
2. Jacobi-Romanovski polynomials possess desirable properties that make them well-suited for PDE applications.
3. A detailed error analysis of the proposed spectral algorithm is provided, which provides valuable insights into the convergence rates of the performance of the proposed technique.
4. Experimental simulations are provided to justify that the recommended approach generates efficient and accurate solutions for the governing fractional-order model.

The structure of the article is as follows: Sect. 2 contains a brief definition of the Jacobi and Jacobi-Romanovski polynomials, which will be used in following sections, along with

an error analysis for the proposed spectral methodology. Section 3 presents the outcome of the novel Jacobi-Romanovski polynomials collocation technique applied to solve the main model. Section 4 is devoted to the computational investigations of the underlying model under diverse scenarios and compares the available outcomes with other relevant research methods. Eventually, the key findings, as well as directions for future research studies, are summarized in Sect. 5.

2 A brief introduction to Jacobi and Jacobi-Romanovski polynomials

This part is devoted to the descriptions of the used basis functions in our proposed spectral algorithm. Initially, we preview some basic facts associated with the Jacobi and Jacobi-Romanovski (JR) polynomials.

2.1 Main ingredient of Jacobi basis functions

The Jacobi polynomials (JPs) play an important role in several branches of mathematics [45]. They are orthogonal and belong to the weight function $w(x) = (1-x)^{\alpha}(1+x)^{\beta}$ on the interval $[-1,1]$ with $\alpha, \beta > -1$. We denote by $J_{\hat{s}}^{\alpha,\beta}(x)$ the $\hat{s}$th degree Jacobi polynomial of order α, β. One of its explicit representation forms for this class of polynomials is given below

$$(1-x)^{\alpha}(1+x)^{\beta} J_{\hat{s}}^{\alpha,\beta}(x) = \frac{(-1)^{\hat{s}}}{2^{\hat{s}}\,\hat{s}!}\frac{d^{\hat{s}}}{dx^{\hat{s}}}\Big[(1-x)^{\hat{s}+\alpha}(1+x)^{\hat{s}+\beta}\Big], \tag{2.1}$$

which is known as the Rodrigues formula for $\hat{s} = 0, 1, 2, \ldots$.

We define next the so-called shifted version of JPs on the interval $[0, L]$, where $L > 0$. With the aid of new change of variable $x \to (-1 + 2x/L)$, we get the shifted JPs (SJPs) denoted by $\mathcal{J}_{\hat{s}}^{\alpha,\beta}(x) := J_{\hat{s}}^{\alpha,\beta}(-1 + 2x/L)$. In the explicit form, we may write the $\hat{s}$-degree SJPs as

$$\mathcal{J}_{\hat{s}}^{\alpha,\beta}(x) := \sum_{s=0}^{\hat{s}} (-1)^{\hat{s}-s} \frac{\Gamma(\hat{s}+s+\alpha+1)\Gamma(\hat{s}+\beta+1)}{\Gamma(\hat{s}+\alpha+\beta+1)\Gamma(s+\beta+1)(\hat{s}-s)!\,s!\,L^{s}}\, x^{s}, \quad \hat{s} \geq 0. \tag{2.2}$$

The orthogonality of SJPs is also deduced against the weight function $w_{\mathcal{J}}(x) \equiv (L-x)^{\alpha} x^{\beta}$. As a result, we have

$$\int_0^L \mathcal{J}_{\hat{s}}^{\alpha,\beta}(x)\, \mathcal{J}_{\hat{r}}^{\alpha,\beta}(x)\, w_{\mathcal{J}}(x) dx = \begin{cases} C_{\hat{s}}, & \text{if } \hat{s} = \hat{r}, \\ 0, & \text{otherwise}, \end{cases} \tag{2.3}$$

where $(2\hat{s}+\alpha+\beta+1)\,\hat{s}!\,\Gamma(\hat{s}+\alpha+\beta+1)\,C_{\hat{s}} := \Gamma(\hat{s}+\alpha+1)\Gamma(\hat{s}+\beta+1)\,L^{\alpha+\beta+1}$. In addition, the ordinary differential equations in which these polynomials are satisfied given by

$$x(L-x)\,y'' + [L(\beta+1) - (\alpha+\beta+2)x]\,y' = -\hat{s}(\hat{s}+\alpha+\beta+1)y,$$

where $y(x) = \mathcal{J}_{\hat{s}}^{\alpha,\beta}(x)$.

2.2 Main ingredient of Romanovski-Jacobi basis functions

A novel set of finite orthogonal bases are the Romanovski-Jacobi (RJ) polynomials. This class was first considered in [46] and then attracted the attention of authors when approximating the solutions of differential equations [47–49]. Let us denote them by $\mathcal{R}_{t}^{\rho,\sigma}(t)$,

which is explicitly rewritten as

$$\mathcal{R}_{\hat{t}}^{\rho,\sigma}(t) := \sum_{\ell=0}^{\hat{t}} (-1)^{\ell} \frac{\Gamma(-\rho-\sigma-\hat{t})\,\Gamma(\rho+\hat{t}+1)}{\ell!\,\Gamma(-\rho-\sigma-\hat{t}-\ell)\,\Gamma(\rho+\ell+1)\,\Gamma(\hat{t}-\ell+1)} t^{\ell}. \tag{2.4}$$

In fact, these are the polynomial solutions of the subsequent Sturm-Liouville problem of singular type

$$\mathcal{L}_{\rho,\sigma}\left(\mathcal{R}_{\hat{t}}^{\rho,\sigma}(t)\right) = \lambda_{\hat{t}}^{\rho,\sigma}\,\mathcal{R}_{\hat{t}}^{\rho,\sigma}(t),$$

where the differential operator $\mathcal{L}_{\rho,\sigma}$ is defined by

$$\begin{aligned}\mathcal{L}_{\rho,\sigma}(\cdot) &= t(t+1)\frac{d^2}{dt^2}(\cdot) + [(\rho+\sigma+2)t + (\rho+1)]\frac{d}{dt}(\cdot)\\ &= t^{-\rho}(1-t)^{-\sigma}\frac{d}{dt}\left[t^{\rho+1}(1+t)^{1+\sigma}\frac{d}{dt}(\cdot)\right],\end{aligned}$$

and the related eigenvalues are given by $\lambda_{\hat{t}}^{\rho,\sigma} = \hat{t}(\hat{t}+\rho+\sigma+1) < 0$.

The next main property of these RJ polynomials is that they are orthogonal against the weight function $w_{RJ}(t) \equiv t^{\rho}(1+t)^{\sigma}$. It is required that $\rho > -1$ and $\sigma < -2N-\rho-1$, where $N > 0$ is a given integer. The domain of orthogonality is over semi-infinite interval $(0,\infty)$. More precisely, we have

$$\int_0^{\infty} \mathcal{R}_{\hat{t}}^{\rho,\sigma}(t)\,\mathcal{R}_{\hat{s}}^{\rho,\sigma}(t)\,w_{RJ}(t)\,dt = \begin{cases}\tilde{C}_{\hat{t}}, & \text{if } \hat{t}=\hat{s},\\ 0, & \text{otherwise,}\end{cases} \tag{2.5}$$

where $\tilde{C}_{\hat{t}} = -\left[\Gamma(\rho+\hat{t}+1)\,\Gamma(-\sigma-\rho-\hat{t})\right] / \left[\hat{t}!\,(\rho+\sigma+2\hat{t}+1)\,\Gamma(-\sigma-\hat{t})\right]$.

For convenience, we shall define the fractional-order (generalized) version of the RJ polynomials. To achieve this aim, we exploit the change of variable $t \to t^{\epsilon}$ in the RJ polynomials $\mathcal{R}_{\hat{t}}^{\rho,\sigma}(t)$. We have

Definition 2.1 The generalized RJ (GRJ) polynomials are defined by the following relation

$$\mathcal{R}_{\hat{t}}^{\rho,\sigma,\epsilon}(t) = \mathcal{R}_{\hat{t}}^{\rho,\sigma}(t^{\epsilon}), \tag{2.6}$$

where $0 < \epsilon \leq 1$ is a real number.

Let us emphasize that by taking $\epsilon = 1$ in (2.6), we retrieve the normal RJ polynomials. The explicit form of GRJ polynomials is easily obtained by relation (2.4). Based on (2.5), we get the associated orthogonality of GRJ polynomials in the form

$$\int_0^{\infty} \mathcal{R}_{\hat{t}}^{\rho,\sigma,\epsilon}(t)\,\mathcal{R}_{\hat{s}}^{\rho,\sigma,\epsilon}(t)\,w_{RJ}^{\epsilon}(t)\,dt = \begin{cases}\tilde{C}_{\hat{t}}^{\epsilon}, & \text{if } \hat{t}=\hat{s},\\ 0, & \text{otherwise,}\end{cases} \tag{2.7}$$

where $\tilde{C}_{\hat{t}}^{\epsilon} = \frac{1}{\epsilon}\tilde{C}_{\hat{t}}$, and the weight function is $w_{RJ}^{\epsilon}(t) = t^{\epsilon-1}w_{RJ}(t^{\epsilon})$.

2.3 Error analysis of product of Jacobi and Romanovski-Jacobi basis functions

To proceed, we set

$$\Omega := \Big\{(x,t) \ : \ x \in [0,L], \quad t \in [0,T]\Big\},$$

where $L \equiv \zeta$ and $T \equiv \lambda$. Let us define the space of weighted $L_2(\Omega)$ in the form

$$\mathbb{V}_W \equiv L_{2,W}(\Omega) := \Big\{\psi : \Omega \to \mathbb{R} \ : \ \psi \text{ is measurable and } \|\psi(x,t)\|_W < \infty\Big\}.$$

Here, the weight function $W(x,t)$ is written as the product of two weight functions $w_{\mathcal{J}}(x)$ and $w^{\epsilon}_{RJ}(t)$ related to SJPs and GRJPs defined above. To be precise, we have $W(x,t) = w_{\mathcal{J}}(x)\, w^{\epsilon}_{RJ}(t)$. The associated norm on this space is defined by

$$\|\Psi(x,t)\|_W := \int_0^L \int_0^T |\Psi(x,t)|^2 \, W(x,t)\, dx\, dt.$$

The subsequent inner product will be assumed on the space $\mathbb{V}_W$

$$\langle \Psi, \Phi \rangle_W := \int_0^L \int_0^T \Psi(x,t)\, \Phi(x,t)\, W(x,t)\, dx\, dt.$$

Let us then consider a subspace of $\mathbb{V}_W$ denoted by $\mathbb{Z}_{\mathcal{S},\mathcal{T}}$ of finite dimension defined by

$$\mathbb{Z}_{\mathcal{S},\mathcal{T}} := \text{Span}\Big\{\mathcal{J}^{\alpha,\beta}_{\hat{s}}(x)\, \mathcal{R}^{\rho,\sigma,\epsilon}_{\hat{t}}(t) \mid \hat{s} = 0,1,\ldots,\mathcal{S},\ \hat{t} = 0,1,\ldots,\mathcal{T}\Big\}. \tag{2.8}$$

It should be stressed that $\mathbb{Z}_{\mathcal{S},\mathcal{T}}$ creates a complete subspace of $\mathbb{V}_W$.

We now suppose that an element $\phi(x,t) \in \mathbb{V}_W$ is approximated by an element of $\mathbb{Z}_{\mathcal{S},\mathcal{T}}$. One says that an element $z_\star(x,t) \in \mathbb{Z}_{\mathcal{S},\mathcal{T}}$ is the nearest (best) approximation to $\phi(x,t)$ if the subsequent relation holds

$$\|\phi - z_\star\|_W = \inf_{\nu \in \mathbb{V}_W} \|\phi - \nu\|_W.$$

See [50, Thm. I1] for the existence of the best approximation. As an ultimate goal, let us denote by $\check{\phi}(x,t) \in \mathbb{Z}_{\mathcal{S},\mathcal{T}}$ the approximate form of $\phi(x,t)$ as the solution of model problem. Therefore, we can write

$$\phi(x,t) \approx \check{\phi}(x,t) := \sum_{\substack{\hat{s}=0,1,\ldots,\mathcal{S} \\ \hat{t}=0,1,\ldots,\mathcal{T}}} \epsilon_{\hat{s},\hat{t}}\, \mathcal{J}^{\alpha,\beta}_{\hat{s}}(x) \mathcal{R}^{\rho,\sigma,\epsilon}_{\hat{t}}(t) = \boldsymbol{J}^T(x)\, \boldsymbol{E}\, \boldsymbol{R}(t), \quad (x,t) \in \Omega, \tag{2.9}$$

where the basis vectors $\boldsymbol{J}(x)$ and $\boldsymbol{R}(t)$, consisting of $(\mathcal{S}+1)$ SJPs and $(\mathcal{T}+1)$ GRJPs, are given respectively by

$$\boldsymbol{J}(x) := \Big[\mathcal{J}^{\alpha,\beta}_0(x) \quad \mathcal{J}^{\alpha,\beta}_1(x) \quad \ldots \quad \mathcal{J}^{\alpha,\beta}_{\mathcal{S}}(x)\Big],$$

$$\boldsymbol{R}(t) := \Big[\mathcal{R}^{\rho,\sigma,\epsilon}_0(t) \quad \mathcal{R}^{\rho,\sigma,\epsilon}_1(t) \quad \ldots \quad \mathcal{R}^{\rho,\sigma,\epsilon}_{\mathcal{T}}(t)\Big],$$

and the matrix $\boldsymbol{E} := (\epsilon_{\hat{s},\hat{t}})^{\mathcal{S},\mathcal{T}}_{\hat{s},\hat{t}=0}$ of size $(\mathcal{S}+1) \times (\mathcal{T}+1)$ contains the unknown coefficients.

We will show that the error between $\phi(x,t)$ and its approximation $\check{\phi}(x,t)$ tends to zero as the number of bases $\mathcal{S}$, $\mathcal{T}$ grows to infinity. So, we define

$$\mathcal{E}_{\mathcal{S},\mathcal{T}}(x,t) := \phi(x,t) - \check{\phi}(x,t). \tag{2.10}$$

When $M := \mathcal{S} = \mathcal{T}$, we represent the error by $\mathcal{E}_M(x,t)$. In this case, we have the following result

Theorem 2.2 *Let $0 < \epsilon \leq 1$ and assume that a continuous function $\phi : \Omega \to \mathbb{R}$ is given and all fractional partial derivatives of $\phi(x,t)$ exist and are continuous on Ω such that all of them of order ϵ bounded by $K_{\epsilon,\phi}$ in magnitude. If $\check{\phi}(x,t) = \boldsymbol{J}^T(x)\,\boldsymbol{E}\,\boldsymbol{R}(t)$ in (2.9) represents the best (nearest) approximation to $\phi(x,t)$ out of $\mathbb{Z}_{\mathcal{S},\mathcal{T}}$ for $M = \mathcal{S} = \mathcal{T}$, then we have*

$$\|\mathcal{E}_M(x,t)\|_W \to 0, \quad \text{as } M \to \infty.$$

Proof Following [51, 52], we can write the generalized Taylor series form of the function $\phi(x,t)$ as follows

$$\begin{aligned}\phi(x,t) &= \sum_{m=0}^{M-1} \frac{1}{\Gamma(1+\epsilon m)} \left(x^{\epsilon} \frac{\partial^{\epsilon}}{\partial x^{\epsilon}} + t^{\epsilon} \frac{\partial^{\epsilon}}{\partial t^{\epsilon}} \right)^m \phi(0^+,0^+) \\ &\quad + \frac{1}{\Gamma(1+\epsilon M)} \left(x^{\epsilon} \frac{\partial^{\epsilon}}{\partial x^{\epsilon}} + t^{\epsilon} \frac{\partial^{\epsilon}}{\partial t^{\epsilon}} \right)^M \phi(\bar{x},\bar{t}), \\ &:= \phi_M(x,t) + R_M(x,t),\end{aligned}$$

where $0 \leq \bar{x} \leq L$ and $0 \leq \bar{t} \leq T$. As a result, we have the next upper bound

$$\begin{aligned}\|R_M(x,t)\|_W^2 &= \frac{1}{\Gamma^2(1+\epsilon M)} \int_0^L \int_0^T \left| \sum_{k=0}^{M} \binom{M}{k} x^{\epsilon k}\, t^{\epsilon(M-k)} \frac{\partial^{\epsilon M} \phi(\bar{x},\bar{t})}{\partial x^{\epsilon k}\, \partial t^{\epsilon(M-k)}} \right|^2 W(x,t)\,dx\,dt \\ &\leq \frac{K_{\epsilon,\phi}^2}{\Gamma^2(1+\epsilon M)} \left\| (x^{\epsilon} + t^{\epsilon})^M \right\|_W^2, \end{aligned} \tag{2.11}$$

where we have assumed that the absolute values of all fractional partial derivatives of $\phi(x,t)$ are bounded by $K_{\epsilon,\phi}$. We now utilize the assumption that the function $\check{\phi}(x,t) = \boldsymbol{J}^T(x)\,\boldsymbol{E}\,\boldsymbol{R}(t)$ given in (2.9) denotes the best approximation to $\phi(x,t)$ out of subspace $\mathbb{Z}_{\mathcal{S},\mathcal{T}}$. As a conclusion, we may write

$$\|\phi(x,t) - \check{\phi}(x,t)\|_W \leq \|\phi(x,t) - \nu(x,t)\|_W, \quad \forall \nu \in \mathbb{V}_W.$$

Let us now substitute $\nu(x,t)$ in the last inequality by $\phi_M(x,t)$ as the Taylor series form of $\phi(x,t)$, which is in $\mathbb{V}_W$. Thus, we can write

$$\begin{aligned}\|\mathcal{E}_M(x,t)\|_W^2 \leq \|R_M(x,t)\|_W^2 &\leq \frac{K_{\epsilon,\phi}^2}{\Gamma^2(1+\epsilon M)} \left\| (x^{\epsilon} + t^{\epsilon})^M \right\|_W^2 \\ &\leq \frac{K_{\epsilon,\phi}^2}{\Gamma^2(1+\epsilon M)} \int_0^L \int_0^T \sum_{k=0}^{2M} \binom{2M}{k} x^{\epsilon k}\, t^{\epsilon(2M-k)}\, w_{\mathcal{J}}(x)\, w_{RJ}^{\epsilon}(t)\,dt\,dx\end{aligned}$$

$$\leq \frac{K_{\epsilon,\phi}^2}{\Gamma^2(1+\epsilon M)} \sum_{k=0}^{2M} \binom{2M}{k} \int_0^L x^{\epsilon k} w_{\mathcal{J}}(x)\, dx \int_0^T t^{\epsilon(2M-k)} w_{RJ}^{\epsilon}(t) dt. \tag{2.12}$$

We next calculate two previous integrals. According to the definitions of weight functions, we have

$$I_{1,k} := \int_0^L x^{\epsilon k} w_{\mathcal{J}}(x)\, dx \leq L^{\alpha} \int_0^L x^{\epsilon k+\beta}\, dx = \frac{L^{\alpha+\epsilon k+\beta+1}}{\epsilon k+\beta+1},$$
$$I_{2,k} := \int_0^T t^{\epsilon(2M-k)} w_{RJ}^{\epsilon}(t)\, dt := \int_0^T t^{\epsilon(2M-k+\rho+1)-1}(1+t^{\epsilon})^{\sigma}\, dt \leq \frac{(1+T^{\epsilon})^{\sigma}\, T^{\epsilon(2M-k+\rho+1)}}{\epsilon(2M-k+\rho+1)}.$$

Let us consider three cases: $k = 0$, $k = 2M$, and $1 \leq k \leq 2M-1$. In the latter case, we immediately reach at the following relation

$$I_{1,k} \times I_{2,k} \leq C_1(M) \left(\frac{L}{T}\right)^{k\epsilon} \frac{1}{k} \times \frac{1}{2M-k} \leq C_1(M) \left(\frac{L}{T}\right)^{k\epsilon}, \quad 1 \leq k \leq 2M-1, \tag{2.13}$$

where $C_1(M) := \frac{1}{\epsilon^2} L^{\alpha+\beta+1} \exp(\sigma\, T^{\epsilon})\, T^{\epsilon(2M+\rho+1)}$. Clearly, for $k = 0$, we have the following inequality

$$I_{1,0} \times I_{2,0} \leq C_2(M) \frac{1}{2M+\rho+1}, \quad C_2(M) := \epsilon\, C_1(M). \tag{2.14}$$

For the case $k = 2M$, we get

$$I_{1,2M} \times I_{2,2M} \leq C_3(M) := \frac{1}{2\epsilon^2 M(\rho+1)} L^{2M\epsilon+\alpha+\beta+1} \exp(\sigma\, T^{\epsilon})\, T^{\epsilon(\rho+1)}. \tag{2.15}$$

Totally, we have

$$\sum_{k=0}^{2M} \binom{2M}{k} I_{1,k} \times I_{2,k} = I_{1,0} \times I_{2,0} + \sum_{k=1}^{2M-1} \binom{2M}{k} I_{1,k} \times I_{2,k} + I_{1,2M} \times I_{2,2M}. \tag{2.16}$$

It remains to estimate an upper bound for the middle term in (2.16). In view of (2.13), we obtain

$$\begin{aligned} \sum_{k=1}^{2M-1} \binom{2M}{k} I_{1,k} \times I_{2,k} &\leq C_1(M) \sum_{k=0}^{2M} \binom{2M}{k} \left(\frac{L}{T}\right)^{k\epsilon} \\ &= C_1(M)\, (1 + L^{\epsilon}/T^{\epsilon})^{2M} \\ &\leq C_1(M) \exp(2ML^{\epsilon}/T^{\epsilon}). \end{aligned} \tag{2.17}$$

The proof is carried out by inserting the three obtained upper bounds (2.14), (2.15), and (2.17) into (2.12) following by approaching M to infinity. □

Remark 2.3 Arguments similar to those described in Theorem 2.2 can be applied in 2D for the error term $\mathcal{E}_M(x,y,t) := \phi(x,y,t) - \breve{\phi}(x,y,t)$ when $M := \mathcal{S} = \mathcal{T} = \mathcal{V}$. In fact, the gen-

eralized Taylor expansion of the function $\phi(x,y,t)$ takes the form

$$\begin{aligned}\phi(x,y,t) &= \sum_{m=0}^{M-1} \frac{1}{\Gamma(1+\epsilon m)} \left(x^{\epsilon} \frac{\partial^{\epsilon}}{\partial x^{\epsilon}} + y^{\epsilon} \frac{\partial^{\epsilon}}{\partial y^{\epsilon}} + t^{\epsilon} \frac{\partial^{\epsilon}}{\partial t^{\epsilon}} \right)^{m} \phi(0^{+},0^{+},0^{+}) \\ &\quad + \frac{1}{\Gamma(1+\epsilon M)} \left(x^{\epsilon} \frac{\partial^{\epsilon}}{\partial x^{\epsilon}} + +y^{\epsilon} \frac{\partial^{\epsilon}}{\partial y^{\epsilon}} + t^{\epsilon} \frac{\partial^{\epsilon}}{\partial t^{\epsilon}} \right)^{M} \phi(\bar{x},\bar{y},\bar{t}), \\ &:= \phi_{M}(x,y,t) + R_{M}(x,y,t),\end{aligned}$$

for some $0 \le \bar{x} \le \zeta_1$, $0 \le \bar{y} \le \zeta_2$, $0 \le \bar{t} \le \lambda$, and the associated space is taken as $\Omega := \Big\{(x,y,t) \,:\, x \in [0,\zeta_1],\ y \in [0,\zeta_2],\ t \in [0,\lambda]\Big\}$.

3 The main aspects of spectral algorithms in 1D and 2D

In the following parts, we are going to develop a spectral collocation algorithm for the one- and two-dimensional time-fractional telegraph equations. The suggested main approach is based on the Romanovski and Jacobi basis functions.

3.1 Time-fractional telegraph equation in 1D

Here, an effective numerical based spectral technique for the time-fractional telegraph equation (TFTE) will be discussed in detail. The following model equation is considered

$$ {}^{LC}\mathbb{D}_{t}^{\omega}\phi(x,t) + {}^{LC}\mathbb{D}_{t}^{\omega-1}\phi(x,t) = c^{2}\Delta\phi(x,t) + \mathcal{N}(x,t), \quad x \in [0,\zeta], \quad t \in [0,\lambda], \tag{3.1}$$

with the subsequent initial and boundary conditions

$$\begin{cases} \phi(0,t) = \chi_1(t), \\ \phi(\zeta,t) = \chi_2(t), \end{cases} \qquad \begin{cases} \phi(x,0) = \chi_3(x), \\ \phi_t(x,0) = \chi_4(x), \end{cases} \tag{3.2}$$

where $\chi_1(t)$, $\chi_2(t)$, $\chi_3(x)$, $\chi_4(x)$, and $\mathcal{N}(x,t)$ are some familiar functions.

The next goal is to combine the shifted Jacobi and shifted Romanovski-Jacobi polynomials in order to express the approximate solution of (3.1) in terms of these functions. To accomplish this task, let us assume that

$$\phi(x,t) \approx \tilde{\phi}(x,t) = \sum_{\substack{\hat{s}=0,1,\ldots,\mathcal{S} \\ \hat{t}=0,1,\ldots,\mathcal{T}}} \epsilon_{\hat{s},\hat{t}}\, \mathcal{J}_{\hat{s}}^{\alpha,\beta}(x)\, \mathcal{R}_{\hat{t}}^{\rho,\sigma,\epsilon}(t), \tag{3.3}$$

where $\epsilon_{\hat{s},\hat{t}}$ are constants to be determined, $\mathcal{J}_{\hat{s}}^{\alpha,\beta}(x)$ is the shifted Jacobi polynomials defined in (2.2), and $\mathcal{R}_{\hat{t}}^{\rho,\sigma,\epsilon}(t)$ is the fractional Romanovski-Jacobi polynomials introduced in (2.6). The integer-order time derivatives are then computed as

$$\frac{\partial\tilde{\phi}}{\partial t} = \sum_{\substack{\hat{s}=0,1,\ldots,\mathcal{S} \\ \hat{t}=0,1,\ldots,\mathcal{T}}} \epsilon_{\hat{s},\hat{t}}\, \mathcal{J}_{\hat{s}}^{\alpha,\beta}(x)\, \mathcal{R}_{\hat{t},1}^{\rho,\sigma,\epsilon}(t), \quad \frac{\partial^{2}\tilde{\phi}}{\partial t^{2}} = \sum_{\substack{\hat{s}=0,1,\ldots,\mathcal{S} \\ \hat{t}=0,1,\ldots,\mathcal{T}}} \epsilon_{\hat{s},\hat{t}}\, \mathcal{J}_{\hat{s}}^{\alpha,\beta}(x)\, \mathcal{R}_{\hat{t},2}^{\rho,\sigma,\epsilon}(t), \tag{3.4}$$

where

$$\mathcal{R}_{\hat{t},j}^{\rho,\sigma,\epsilon}(t) := \frac{\partial^{j}}{\partial t^{j}} \mathcal{R}_{\hat{t}}^{\rho,\sigma,\epsilon}(t), \quad j = 1,2. \tag{3.5}$$

Moreover, the integer-order spatial derivatives are

$$\frac{\partial\tilde{\phi}}{\partial x}=\sum_{\substack{\hat{s}=0,1,\ldots,\mathcal{S}\\ \hat{t}=0,1,\ldots,\mathcal{T}}}\epsilon_{\hat{s},\hat{t}}\,\mathcal{J}_{\hat{s},1}^{\alpha,\beta}(x)\,\mathcal{R}_{\hat{t}}^{\rho,\sigma,\epsilon}(t),\qquad \frac{\partial^2\tilde{\phi}}{\partial x^2}=\sum_{\substack{\hat{s}=0,1,\ldots,\mathcal{S}\\ \hat{t}=0,1,\ldots,\mathcal{T}}}\epsilon_{\hat{s},\hat{t}}\,\mathcal{J}_{\hat{s},2}^{\alpha,\beta}(x)\,\mathcal{R}_{\hat{t}}^{\rho,\sigma,\epsilon}(t), \tag{3.6}$$

where

$$\mathcal{J}_{\hat{s},j}^{\alpha,\beta}(x):=\frac{\partial^j}{\partial x^j}\mathcal{J}_{\hat{s}}^{\alpha,\beta}(x),\quad j=1,2. \tag{3.7}$$

Additionally, we can expand the Liouville-Caputo fractional derivatives ${}^{LC}\mathbb{D}_t^{\eta}\tilde{\phi}(x,t)$ of orders $\eta=\omega,\omega-1$ in the forms

$$\begin{aligned}{}^{LC}\mathbb{D}_t^{\eta}\,\tilde{\phi}(x,t)&=\sum_{\substack{\hat{s}=0,1,\ldots,\mathcal{S}\\ \hat{t}=0,1,\ldots,\mathcal{T}}}\epsilon_{\hat{s},\hat{t}}\,\mathcal{J}_{\hat{s}}^{\alpha,\beta}(x)\,{}^{LC}\mathbb{D}_t^{\eta}(\mathcal{R}_{\hat{t}}^{\rho,\sigma,\epsilon}(t))\\&=\sum_{\substack{\hat{s}=0,1,\ldots,\mathcal{S}\\ \hat{t}=0,1,\ldots,\mathcal{T}}}\epsilon_{\hat{s},\hat{t}}\,\mathcal{J}_{\hat{s}}^{\alpha,\beta}(x)\,\mathcal{R}_{\hat{t},\eta}^{\rho,\sigma,\epsilon}(t),\end{aligned} \tag{3.8}$$

we have used the notations $\mathcal{R}_{\hat{t},\eta}^{\rho,\sigma,\epsilon}(t):={}^{LC}\mathbb{D}_t^{\eta}\left(\mathcal{R}_{\hat{t}}^{\rho,\sigma,\epsilon}(t)\right)$ for $\eta=\omega,\omega-1$. Here,

$$\mathcal{R}_{\hat{t},\eta}^{\rho,\sigma,\epsilon}(t)=\frac{1}{\Gamma(k-\eta)}\int_0^t\frac{1}{(t-\tau)^{\eta-k+1}}\frac{d^k}{d\tau^k}(\mathcal{R}_{\hat{t}}^{\rho,\sigma,\epsilon}(\tau))\,d\tau,\quad k-1<\eta<k, \tag{3.9}$$

where $\Gamma(\cdot)$ denotes the Gamma function.

Remark 3.1 We can expand the Liouville-Caputo fractional derivatives $\mathcal{R}_{\hat{t},\eta}^{\rho,\sigma,\epsilon}(t)$ of order $\eta=\omega,\omega-1$ in the forms

$$\mathcal{R}_{\hat{t},\eta}^{\rho,\sigma,\epsilon}(t)=\sum_{\ell=k}^{\hat{t}}(-1)^{\ell}\frac{\Gamma(-\rho-\sigma-\hat{t})\,\Gamma(\rho+\hat{t}+1)}{\ell!\,\Gamma(-\rho-\sigma-\hat{t}-\ell)\,\Gamma(\rho+\ell+1)\,\Gamma(\hat{t}-\ell+1)}\frac{\Gamma(\epsilon\,\ell+1)t^{\ell\,\epsilon-\eta}}{\Gamma(\epsilon\,\ell-\eta+1)}. \tag{3.10}$$

By substituting the preceding relations (3.3)–(3.8) into the main one-dimensional TFTE (3.1), we get

$$\begin{aligned}\sum_{\substack{\hat{s}=0,1,\ldots,\mathcal{S}\\ \hat{t}=0,1,\ldots,\mathcal{T}}}\epsilon_{\hat{s},\hat{t}}\,\mathcal{J}_{\hat{s}}^{\alpha,\beta}(x)\left(\mathcal{R}_{\hat{t},\omega}^{\rho,\sigma,\epsilon}(t)+\mathcal{R}_{\hat{t},\omega-1}^{\rho,\sigma,\epsilon}(t)\right)&=c^2\left(\sum_{\substack{\hat{s}=0,1,\ldots,\mathcal{S}\\ \hat{t}=0,1,\ldots,\mathcal{T}}}\epsilon_{\hat{s},\hat{t}}\mathcal{J}_{\hat{s},2}^{\alpha,\beta}(x)\,\mathcal{R}_{\hat{t}}^{\rho,\sigma,\epsilon}(t)\right)\\&\quad+\mathcal{N}(x,t).\end{aligned} \tag{3.11}$$

Besides, the provided initial and boundary conditions (3.2) can be written as

$$\begin{cases}\sum_{\substack{\hat{s}=0,1,\ldots,\mathcal{S}\\ \hat{t}=0,1,\ldots,\mathcal{T}}}\epsilon_{\hat{s},\hat{t}}\,\mathcal{J}_{\hat{s}}^{\alpha,\beta}(0)\,\mathcal{R}_{\hat{t}}^{\rho,\sigma,\epsilon}(t)=\chi_1(t),\\ \sum_{\substack{\hat{s}=0,1,\ldots,\mathcal{S}\\ \hat{t}=0,1,\ldots,\mathcal{T}}}\epsilon_{\hat{s},\hat{t}}\,\mathcal{J}_{\hat{s}}^{\alpha,\beta}(\zeta)\,\mathcal{R}_{\hat{t}}^{\rho,\sigma,\epsilon}(t)=\chi_2(t),\end{cases}\qquad\begin{cases}\sum_{\substack{\hat{s}=0,1,\ldots,\mathcal{S}\\ \hat{t}=0,1,\ldots,\mathcal{T}}}\epsilon_{\hat{s},\hat{t}}\,\mathcal{J}_{\hat{s}}^{\alpha,\beta}(x)\,\mathcal{R}_{\hat{t}}^{\rho,\sigma,\epsilon}(0)=\chi_3(x),\\ \sum_{\substack{\hat{s}=0,1,\ldots,\mathcal{S}\\ \hat{t}=0,1,\ldots,\mathcal{T}}}\epsilon_{\hat{s},\hat{t}}\,\mathcal{J}_{\hat{s}}^{\alpha,\beta}(x)\,\mathcal{R}_{\hat{t},1}^{\rho,\sigma,\epsilon}(0)=\chi_4(x).\end{cases} \tag{3.12}$$

To proceed, we require a set of $(\mathcal{S}+1)\times(\mathcal{T}+1)$ collocation points to obtain the unknown coefficients $\epsilon_{\hat{s},\hat{t}}$ in (3.3). To achieve this goal, the Romanovski-Jacobi-Gauss-Radau nodes $\{t_i\}_{i=1}^{\mathcal{T}}$ are the zeros of $\mathcal{R}_{\hat{t}}^{\rho+1,\sigma}$ and $t_0=0$, whenever, the Jacobi-Gauss-Lobatto nodes $\{x_j\}_{j=1}^{\mathcal{S}-1}$ are the zeros of $\frac{d}{dx}(\mathcal{J}_{\hat{s}}^{\alpha,\beta}(x))$ and $x_0=0$, $x_{\mathcal{S}}=\zeta$.

We now evaluate the set of equations (3.11) and (3.12) at the former selected collocation nodes. The resulting algebraic system of equations is obtained as follows

$$\begin{aligned}\sum_{\substack{\hat{s}=0,1,\ldots,\mathcal{S}\\ \hat{t}=0,1,\ldots,\mathcal{T}}}\epsilon_{\hat{s},\hat{t}}\,\mathcal{J}_{\hat{s}}^{\alpha,\beta}(x_i)\Big(\mathcal{R}_{\hat{t},\omega}^{\rho,\sigma,\epsilon}(t_j)+\mathcal{R}_{\hat{t},\omega-1}^{\rho,\sigma,\epsilon}(t_j)\Big)=&c^2\Big(\sum_{\substack{\hat{s}=0,1,\ldots,\mathcal{S}\\ \hat{t}=0,1,\ldots,\mathcal{T}}}\epsilon_{\hat{s},\hat{t}}\,\mathcal{J}_{\hat{s},2}^{\alpha,\beta}(x_i)\mathcal{R}_{\hat{t}}^{\rho,\sigma,\epsilon}(t_j)\Big)\\ &+\mathcal{N}(x_i,t_j),\end{aligned}\tag{3.13}$$

and

$$\begin{cases}\sum_{\substack{\hat{s}=0,1,\ldots,\mathcal{S}\\ \hat{t}=0,1,\ldots,\mathcal{T}}}\epsilon_{\hat{s},\hat{t}}\,\mathcal{J}_{\hat{s}}^{\alpha,\beta}(0)\,\mathcal{R}_{\hat{t}}^{\rho,\sigma,\epsilon}(t_j)=\chi_1(t_j),\\ \sum_{\substack{\hat{s}=0,1,\ldots,\mathcal{S}\\ \hat{t}=0,1,\ldots,\mathcal{T}}}\epsilon_{\hat{s},\hat{t}}\,\mathcal{J}_{\hat{s}}^{\alpha,\beta}(\zeta)\,\mathcal{R}_{\hat{t}}^{\rho,\sigma,\epsilon}(t_j)=\chi_2(t_j),\end{cases}\qquad\begin{cases}\sum_{\substack{\hat{s}=0,1,\ldots,\mathcal{S}\\ \hat{t}=0,1,\ldots,\mathcal{T}}}\epsilon_{\hat{s},\hat{t}}\,\mathcal{J}_{\hat{s}}^{\alpha,\beta}(x_i)\,\mathcal{R}_{\hat{t}}^{\rho,\sigma,\epsilon}(0)=\chi_3(x_i)\\ \sum_{\substack{\hat{s}=0,1,\ldots,\mathcal{S}\\ \hat{t}=0,1,\ldots,\mathcal{T}}}\epsilon_{\hat{s},\hat{t}}\,\mathcal{J}_{\hat{s}}^{\alpha,\beta}(x_i)\,\mathcal{R}_{\hat{t},1}^{\rho,\sigma,\epsilon}(0)=\chi_4(x_i).\end{cases}\tag{3.14}$$

After solving the above system of equations (3.13)–(3.14), we get the unknown coefficients $\epsilon_{\hat{s},\hat{t}}$ for $\hat{s}=0,1,\ldots,\mathcal{S}$ and $\hat{t}=0,1,\ldots,\mathcal{T}$.

3.2 The time-fractional telegraph equation in 2D

Now, we consider the two-dimensional TFTE. This model equation has the following form

$$\begin{aligned}&{}^{LC}\mathbb{D}_t^{\omega}\,\phi(x,y,t)+{}^{LC}\mathbb{D}_t^{\omega-1}\,\phi(x,y,t)=c^2\,\Delta\,\phi(x,y,t)+\mathcal{N}(x,y,t),\\ &\quad x\in[0,\zeta_1],\ y\in[0,\zeta_2],\ t\in[0,\lambda].\end{aligned}\tag{3.15}$$

The following initial and boundary conditions are

$$\begin{cases}\phi(0,y,t)=\chi_1(y,t),\\ \phi(\zeta_1,y,t)=\chi_2(y,t),\end{cases}\qquad\begin{cases}\phi(x,0,t)=\chi_3(x,t),\\ \phi(x,\zeta_2,t)=\chi_4(x,t),\end{cases}\qquad\begin{cases}\phi(x,y,0)=\chi_5(x,y),\\ \phi_t(x,y,0)=\chi_6(x,y).\end{cases}\tag{3.16}$$

Here, the functions $\chi_1(y,t)$, $\chi_2(y,t)$, $\chi_3(y,t)$, $\chi_4(x,t)$, $\chi_5(x,y)$, $\chi_6(x,y)$, and $\mathcal{N}(x,y,t)$ are known.

Let the approximate solution of (3.15) be denoted by $\tilde{\phi}(x,y,t)\approx\phi(x,y,t)$. Similar to one-dimensional problem, we may expand $\tilde{\phi}(x,y,t)$ as a combination of shifted Jacobi functions and the shifted version of Romanovski-Jacobi polynomials. Let us express the approximate solution in the form

$$\tilde{\phi}(x,y,t)=\sum_{\substack{\hat{s}=0,1,\ldots,\mathcal{S}\\ \hat{v}=0,1,\ldots,\mathcal{V}\\ \hat{t}=0,1,\ldots,\mathcal{T}}}\epsilon_{\hat{s},\hat{v},\hat{t}}\,\mathcal{J}_{\hat{s}}^{\alpha_1,\beta_1}(x)\,\mathcal{J}_{\hat{v}}^{\alpha_2,\beta_2}(y)\,\mathcal{R}_{\hat{t}}^{\rho,\sigma,\epsilon}(t),\tag{3.17}$$

where $\mathcal{J}_{\hat{s}}^{\alpha_i,\beta_i}(x)$ for $i = 1,2$ represent the shifted Jacobi polynomials defined in (2.2). Furthermore, the third basis $\mathcal{R}_{\hat{t}}^{\rho,\sigma,\epsilon}(t)$ denotes the generalized Romanovski-Jacobi polynomials defined by (2.6).

Let us calculate the integer-order time derivatives of $\tilde{\phi}(x,y,t)$. To this end, we use the notations defined in (3.5). Therefore, we obtain

$$\begin{aligned}
\frac{\partial\tilde{\phi}}{\partial t} &= \sum_{\substack{\hat{s}=0,1,\ldots,\mathcal{S}\\ \hat{\nu}=0,1,\ldots,\mathcal{V}\\ \hat{t}=0,1,\ldots,\mathcal{T}}} \epsilon_{\hat{s},\hat{\nu},\hat{t}}\,\mathcal{J}_{\hat{s}}^{\alpha_1,\beta_1}(x)\,\mathcal{J}_{\hat{\nu}}^{\alpha_2,\beta_2}(y)\,\mathcal{R}_{\hat{t},1}^{\rho,\sigma,\epsilon}(t),\\
\frac{\partial^2\tilde{\phi}}{\partial t^2} &= \sum_{\substack{\hat{s}=0,1,\ldots,\mathcal{S}\\ \hat{\nu}=0,1,\ldots,\mathcal{V}\\ \hat{t}=0,1,\ldots,\mathcal{T}}} \epsilon_{\hat{s},\hat{\nu},\hat{t}}\,\mathcal{J}_{\hat{s}}^{\alpha_1,\beta_1}(x)\,\mathcal{J}_{\hat{\nu}}^{\alpha_2,\beta_2}(y)\,\mathcal{R}_{\hat{t},2}^{\rho,\sigma,\epsilon}(t).
\end{aligned} \tag{3.18}$$

By utilizing the symbols defined in (3.7), the integer-order spatial derivatives with respect to x are computed as

$$\begin{aligned}
\frac{\partial\tilde{\phi}}{\partial x} &= \sum_{\substack{\hat{s}=0,1,\ldots,\mathcal{S}\\ \hat{\nu}=0,1,\ldots,\mathcal{V}\\ \hat{t}=0,1,\ldots,\mathcal{T}}} \epsilon_{\hat{s},\hat{\nu},\hat{t}}\,\mathcal{J}_{\hat{s},1}^{\alpha_1,\beta_1}(x)\,\mathcal{J}_{\hat{\nu}}^{\alpha_2,\beta_2}(y)\,\mathcal{R}_{\hat{t}}^{\rho,\sigma,\epsilon}(t),\\
\frac{\partial^2\tilde{\phi}}{\partial x^2} &= \sum_{\substack{\hat{s}=0,1,\ldots,\mathcal{S}\\ \hat{\nu}=0,1,\ldots,\mathcal{V}\\ \hat{t}=0,1,\ldots,\mathcal{T}}} \epsilon_{\hat{s},\hat{\nu},\hat{t}}\,\mathcal{J}_{\hat{s},2}^{\alpha_1,\beta_1}(x)\,\mathcal{J}_{\hat{\nu}}^{\alpha_2,\beta_2}(y)\,\mathcal{R}_{\hat{t}}^{\rho,\sigma,\epsilon}(t).
\end{aligned} \tag{3.19}$$

Analogously, by defining $\mathcal{J}_{\hat{\nu},j}^{\alpha_2,\beta_2}(y) := \frac{\partial^j}{\partial y^j}\mathcal{J}_{\hat{\nu}}^{\alpha_2,\beta_2}(y)$ for $j = 1,2$, we may express the integer-order spatial derivatives with respect to y as

$$\begin{aligned}
\frac{\partial\tilde{\phi}}{\partial y} &= \sum_{\substack{\hat{s}=0,1,\ldots,\mathcal{S}\\ \hat{\nu}=0,1,\ldots,\mathcal{V}\\ \hat{t}=0,1,\ldots,\mathcal{T}}} \epsilon_{\hat{s},\hat{\nu},\hat{t}}\,\mathcal{J}_{\hat{s}}^{\alpha_1,\beta_1}(x)\,\mathcal{J}_{\hat{\nu},1}^{\alpha_2,\beta_2}(y)\,\mathcal{R}_{\hat{t}}^{\rho,\sigma,\epsilon}(t),\\
\frac{\partial^2\tilde{\phi}}{\partial y^2} &= \sum_{\substack{\hat{s}=0,1,\ldots,\mathcal{S}\\ \hat{\nu}=0,1,\ldots,\mathcal{V}\\ \hat{t}=0,1,\ldots,\mathcal{T}}} \epsilon_{\hat{s},\hat{\nu},\hat{t}}\,\mathcal{J}_{\hat{s}}^{\alpha_1,\beta_1}(x)\,\mathcal{J}_{\hat{\nu},2}^{\alpha_2,\beta_2}(y)\mathcal{R}_{\hat{t}}^{\rho,\sigma,\epsilon}(t).
\end{aligned} \tag{3.20}$$

It remains to compute the Liouville-Caputo derivatives ${}^{LC}\mathbb{D}_t^{\eta}\,\tilde{\phi}(x,y,t)$ for $\eta = \omega, \omega-1$. In view of $\mathcal{R}_{\hat{t},\eta}^{\rho,\sigma,\epsilon}(t) := {}^{LC}\mathbb{D}_t^{\eta}\left(\mathcal{R}_{\hat{t}}^{\rho,\sigma,\epsilon}(t)\right)$ for $\eta = \omega, \omega-1$ and Remark 3.1, we get

$${}^{LC}\mathbb{D}_t^{\eta}\,\tilde{\phi}(x,y,t) = \sum_{\substack{\hat{s}=0,1,\ldots,\mathcal{S}\\ \hat{\nu}=0,1,\ldots,\mathcal{V}\\ \hat{t}=0,1,\ldots,\mathcal{T}}} \epsilon_{\hat{s},\hat{\nu},\hat{t}}\,\mathcal{J}_{\hat{s}}^{\alpha_1,\beta_1}(x)\,\mathcal{J}_{\hat{\nu}}^{\alpha_2,\beta_2}(y)\,\mathcal{R}_{\hat{t},\eta}^{\rho,\sigma,\epsilon}(t), \quad \eta = \omega, \omega-1. \tag{3.21}$$

All the obtained relations (3.17)–(3.21) will now be inserted into (3.15). The resulting relation is as follows

$$\sum_{\substack{\hat{s}=0,1,\ldots,\mathcal{S}\\ \hat{\nu}=0,1,\ldots,\mathcal{V}\\ \hat{t}=0,1,\ldots,\mathcal{T}}} \epsilon_{\hat{s},\hat{\nu},\hat{t}}\,\mathcal{J}_{\hat{s}}^{\alpha_1,\beta_1}(x)\,\mathcal{J}_{\hat{\nu}}^{\alpha_2,\beta_2}(y)\left(\mathcal{R}_{\hat{t},\omega}^{\rho,\sigma,\epsilon}(t) + \mathcal{R}_{\hat{t},\omega-1}^{\rho,\sigma,\epsilon}(t)\right) = \mathcal{Q}(x,y,t), \tag{3.22}$$

where

$$\mathcal{Q}(x,y,t) = c^2\Bigg(\sum_{\substack{\hat{s}=0,1,\ldots,\mathcal{S}\\ \hat{\nu}=0,1,\ldots,\mathcal{V}\\ \hat{t}=0,1,\ldots,\mathcal{T}}} \epsilon_{\hat{s},\hat{\nu},\hat{t}}\Big(\mathcal{J}_{\hat{s},2}^{\alpha_1,\beta_1}(x)\,\mathcal{J}_{\hat{\nu}}^{\alpha_2,\beta_2}(y) + \mathcal{J}_{\hat{s}}^{\alpha_1,\beta_1}(x)\,\mathcal{J}_{\hat{\nu},2}^{\alpha_2,\beta_2}(y)\Big)\mathcal{R}_{\hat{t},2}^{\rho,\sigma,\epsilon}(t)\Bigg) + \mathcal{N}(x,y,t).$$

In addition, the given initial and boundary conditions (3.16) are converted to

$$\begin{cases} \sum_{\substack{\hat{s}=0,1,\ldots,\mathcal{S}\\ \hat{\nu}=0,1,\ldots,\mathcal{V}\\ \hat{t}=0,1,\ldots,\mathcal{T}}} \epsilon_{\hat{s},\hat{\nu},\hat{t}}\,\mathcal{J}_{\hat{s}}^{\alpha_1,\beta_1}(0)\,\mathcal{J}_{\hat{\nu}}^{\alpha_2,\beta_2}(y)\,\mathcal{R}_{\hat{t}}^{\rho,\sigma,\epsilon}(t) = \chi_1(y,t),\\ \sum_{\substack{\hat{s}=0,1,\ldots,\mathcal{S}\\ \hat{\nu}=0,1,\ldots,\mathcal{V}\\ \hat{t}=0,1,\ldots,\mathcal{T}}} \epsilon_{\hat{s},\hat{\nu},\hat{t}}\,\mathcal{J}_{\hat{s}}^{\alpha_1,\beta_1}(\zeta_1)\,\mathcal{J}_{\hat{\nu}}^{\alpha_2,\beta_2}(y)\,\mathcal{R}_{\hat{t}}^{\rho,\sigma,\epsilon}(t) = \chi_2(y,t), \end{cases}$$

$$\begin{cases} \sum_{\substack{\hat{s}=0,1,\ldots,\mathcal{S}\\ \hat{\nu}=0,1,\ldots,\mathcal{V}\\ \hat{t}=0,1,\ldots,\mathcal{T}}} \epsilon_{\hat{s},\hat{\nu},\hat{t}}\,\mathcal{J}_{\hat{s}}^{\alpha_1,\beta_1}(x)\,\mathcal{J}_{\hat{\nu}}^{\alpha_2,\beta_2}(0)\,\mathcal{R}_{\hat{t}}^{\rho,\sigma,\epsilon}(t) = \chi_3(x,t),\\ \sum_{\substack{\hat{s}=0,1,\ldots,\mathcal{S}\\ \hat{\nu}=0,1,\ldots,\mathcal{V}\\ \hat{t}=0,1,\ldots,\mathcal{T}}} \epsilon_{\hat{s},\hat{\nu},\hat{t}}\,\mathcal{J}_{\hat{s}}^{\alpha_1,\beta_1}(x)\,\mathcal{J}_{\hat{\nu}}^{\alpha_2,\beta_2}(\zeta_2)\,\mathcal{R}_{\hat{t}}^{\rho,\sigma,\epsilon}(t) = \chi_4(x,t), \end{cases} \tag{3.23}$$

$$\begin{cases} \sum_{\substack{\hat{s}=0,1,\ldots,\mathcal{S}\\ \hat{\nu}=0,1,\ldots,\mathcal{V}\\ \hat{t}=0,1,\ldots,\mathcal{T}}} \epsilon_{\hat{s},\hat{\nu},\hat{t}}\,\mathcal{J}_{\hat{s}}^{\alpha_1,\beta_1}(x)\,\mathcal{J}_{\hat{\nu}}^{\alpha_2,\beta_2}(y)\,\mathcal{R}_{\hat{t}}^{\rho,\sigma,\epsilon}(0) = \chi_5(x,y),\\ \sum_{\substack{\hat{s}=0,1,\ldots,\mathcal{S}\\ \hat{\nu}=0,1,\ldots,\mathcal{V}\\ \hat{t}=0,1,\ldots,\mathcal{T}}} \epsilon_{\hat{s},\hat{\nu},\hat{t}}\,\mathcal{J}_{\hat{s}}^{\alpha_1,\beta_1}(x)\,\mathcal{J}_{\hat{\nu}}^{\alpha_2,\beta_2}(y)\,\mathcal{R}_{\hat{t},1}^{\rho,\sigma,\epsilon}(0) = \chi_6(x,y). \end{cases}$$

A set of $(\mathcal{S}+1)\times(\mathcal{V}+1)\times(\mathcal{T}+1)$ collocation nodes will be needed to determine the unknown coefficients $\epsilon_{\hat{s},\hat{\nu},\hat{t}}$ in (3.17). To achieve this goal, the Romanovski-Jacobi-Gauss-Radau nodes $\{t_i\}_{i=1}^{\mathcal{T}}$ are the zeros of $\mathcal{R}_{\hat{t}}^{\rho+1,\sigma}$ and $t_0 = 0$, whenever, the Jacobi-Gauss-Lobatto nodes $\{x_j\}_{j=1}^{\mathcal{S}-1}$ are the zeros of $\frac{d}{dx}(\mathcal{J}_{\hat{s}}^{\alpha,\beta}(x))$, and $x_0 = 0$, $x_{\mathcal{S}} = \zeta_1$ and the Jacobi-Gauss-Lobatto nodes $\{y_k\}_{k=1}^{\mathcal{V}-1}$ are the zeros of $\frac{d}{dy}(\mathcal{J}_{\hat{\nu}}^{\alpha_2,\beta_2}(y))$ and $y_0 = 0$, $y_{\mathcal{V}} = \zeta_2$.

We then collocate the relations (3.22) and (3.23) at the collocation nodes and get

$$\sum_{\substack{\hat{s}=0,1,\ldots,\mathcal{S}\\ \hat{\nu}=0,1,\ldots,\mathcal{V}\\ \hat{t}=0,1,\ldots,\mathcal{T}}} \epsilon_{\hat{s},\hat{\nu},\hat{t}}\,\mathcal{J}_{\hat{s}}^{\alpha_1,\beta_1}(x_i)\,\mathcal{J}_{\hat{\nu}}^{\alpha_2,\beta_2}(y_j)\Big(\mathcal{R}_{\hat{t},\omega}^{\rho,\sigma,\epsilon}(t_k) + \mathcal{R}_{\hat{t},\omega-1}^{\rho,\sigma,\epsilon}(t_k)\Big) = \mathcal{Q}(x_i,y_j,t_k), \tag{3.24}$$

and

$$\begin{cases} \sum_{\substack{\hat{s}=0,1,\ldots,\mathcal{S}\\ \hat{\nu}=0,1,\ldots,\mathcal{V}\\ \hat{t}=0,1,\ldots,\mathcal{T}}} \epsilon_{\hat{s},\hat{\nu},\hat{t}}\,\mathcal{J}_{\hat{s}}^{\alpha_1,\beta_1}(0)\,\mathcal{J}_{\hat{\nu}}^{\alpha_2,\beta_2}(y_j)\,\mathcal{R}_{\hat{t}}^{\rho,\sigma,\epsilon}(t_k) = \chi_1(y_j,t_k),\\ \sum_{\substack{\hat{s}=0,1,\ldots,\mathcal{S}\\ \hat{\nu}=0,1,\ldots,\mathcal{V}\\ \hat{t}=0,1,\ldots,\mathcal{T}}} \epsilon_{\hat{s},\hat{\nu},\hat{t}}\,\mathcal{J}_{\hat{s}}^{\alpha_1,\beta_1}(\zeta_1)\,\mathcal{J}_{\hat{\nu}}^{\alpha_2,\beta_2}(y_j)\,\mathcal{R}_{\hat{t}}^{\rho,\sigma,\epsilon}(t_k) = \chi_2(y_j,t_k), \end{cases}$$

$$\begin{cases} \sum_{\substack{\hat{s}=0,1,\ldots,\mathcal{S}\\ \hat{\nu}=0,1,\ldots,\mathcal{V}\\ \hat{t}=0,1,\ldots,\mathcal{T}}} \epsilon_{\hat{s},\hat{\nu},\hat{t}}\,\mathcal{J}_{\hat{s}}^{\alpha_1,\beta_1}(x_i)\,\mathcal{J}_{\hat{\nu}}^{\alpha_2,\beta_2}(0)\,\mathcal{R}_{\hat{t}}^{\rho,\sigma,\epsilon}(t_k) = \chi_3(x_i,t_k),\\ \sum_{\substack{\hat{s}=0,1,\ldots,\mathcal{S}\\ \hat{\nu}=0,1,\ldots,\mathcal{V}\\ \hat{t}=0,1,\ldots,\mathcal{T}}} \epsilon_{\hat{s},\hat{\nu},\hat{t}}\,\mathcal{J}_{\hat{s}}^{\alpha_1,\beta_1}(x_i)\,\mathcal{J}_{\hat{\nu}}^{\alpha_2,\beta_2}(\zeta_2)\,\mathcal{R}_{\hat{t}}^{\rho,\sigma,\epsilon}(t_k) = \chi_4(x_i,t_k), \end{cases} \tag{3.25}$$

$$\begin{cases} \sum_{\substack{\hat{s}=0,1,\ldots,\mathcal{S}\\ \hat{v}=0,1,\ldots,\mathcal{V}\\ \hat{t}=0,1,\ldots,\mathcal{T}}} \epsilon_{\hat{s},\hat{v},\hat{t}}\, \mathcal{J}_{\hat{s}}^{\alpha_1,\beta_1}(x_i)\, \mathcal{J}_{\hat{v}}^{\alpha_2,\beta_2}(y_j)\, \mathcal{R}_{\hat{t}}^{\rho,\sigma,\epsilon}(0) = \chi_5(x_i,y_j), \\ \sum_{\substack{\hat{s}=0,1,\ldots,\mathcal{S}\\ \hat{v}=0,1,\ldots,\mathcal{V}\\ \hat{t}=0,1,\ldots,\mathcal{T}}} \epsilon_{\hat{s},\hat{v},\hat{t}}\, \mathcal{J}_{\hat{s}}^{\alpha_1,\beta_1}(x_i)\, \mathcal{J}_{\hat{v}}^{\alpha_2,\beta_2}(y_j)\, \mathcal{R}_{\hat{t},1}^{\rho,\sigma,\epsilon}(0) = \chi_6(x_i,y_j). \end{cases}$$

The above system of algebraic equations (3.24) and (3.25) must be solved to give us the unknown coefficients $\epsilon_{\hat{s},\hat{v},\hat{t}}$ in the expansion series (3.17).

4 Computational evidences

The utility and applicability of the recommended spectral collocation technique are illustrated in the following part. In order to measure the error, we calculate the difference between the estimated and exact solutions through the following formulae

$$E(x,t) = |\phi(x,t) - \tilde{\phi}(x,t)|, \quad \text{and} \quad E(x,y,t) = |\phi(x,y,t) - \tilde{\phi}(x,y,t)|, \tag{4.1}$$

in one- and two-dimensional cases. Here, ϕ denotes the true solution while $\tilde{\phi}$ is the corresponding approximated solution of the models. The greatest absolute values of the errors are denoted by L_∞. These are defined by

$$L_\infty := \max_{(x,t)\in[0,\zeta]\times[0,\lambda]} E(x,t), \quad L_\infty := \max_{(x,y,t)\in[0,\zeta_1]\times[0,\zeta_2]\times[0,\lambda]} E(x,y,t). \tag{4.2}$$

Note that in the next examples we take $\epsilon = 1$, furthermore for nonsmooth solutions we can use the same analysis with fractional values of ϵ, which give us very accurate results.

Example 4.1 We take the following TFTE (3.1) in 1D given by

$$\begin{aligned} {}^{LC}\mathbb{D}_t^{\omega}\phi(x,t) + {}^{LC}\mathbb{D}_t^{\omega-1}\phi(x,t) + \phi(x,t) = \frac{1}{2}t^3\Big[12\sin^2(x)\left(\frac{t^{-\omega}}{\Gamma(4-\omega)} + \frac{t^{1-\omega}}{\Gamma(5-\omega)}\right) \\ - 5\cos(2x) + 1\Big] + \Delta\phi(x,t), \end{aligned} \tag{4.3}$$

where $\zeta = \lambda = 1$. The associated initial and boundary conditions (3.2) are extracted from the actual true solution $\phi(x,t) = t^3\sin^2(x)$. Furthermore, the following four cases for the parameters related to the basis functions and the fractional order ω are taken

1. Case I: $\alpha,\beta = 0$, $\omega = 1.5$, $\rho = 1$, $\sigma = -30$.
2. Case II: $\alpha,\beta = 0$, $\omega = 1.5$, $\rho = 3$, $\sigma = -50$.
3. Case III: $\alpha,\beta = 0$, $\omega = 1.9$, $\rho = 4$, $\sigma = -40$.
4. Case IV: $\alpha,\beta = 0$, $\omega = 1.9$, $\rho = 6$, $\sigma = -80$.

To begin computations, we first consider Case I. We also set $\mathcal{S},\mathcal{T} = 10$. The graphs of approximate solution $\tilde{\phi}(x,t)$ together with the related achieved absolute errors $E(x,t)$ are visualized in Fig. 1.

To show the superiority of presented spectral collocation algorithm, we compare the achieved absolute error and the root mean square (RMS) error in Table 1 and Table 2. The comparisons have been made between the results obtained using our technique and those obtained using the local meshless scheme (LMS) [53]. It is evident that our results with less computational effort are more accurate in comparison with the LMS.

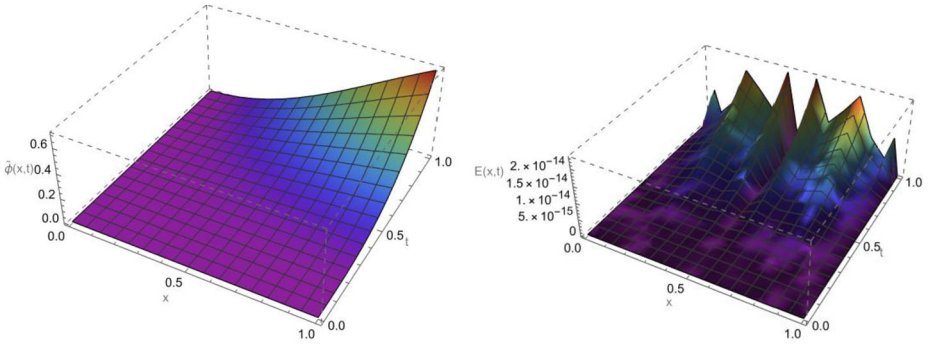

Figure 1 The approximate solution $\tilde{\phi}(x,t)$ (left) and the attained absolute errors (right) for Example 4.1, for Case I with $\mathcal{S},\mathcal{T}=10$

Table 1 The results of L_∞ and L_{rms} for Example 4.1 reported in [53]

δt	$M=501, m=3$				m	$M,N=1000$	
	$\omega=1.5$		$\omega=1.9$			$\omega=1.9$	
	L_∞	L_{rms}	L_∞	L_{rms}		L_∞	L_{rms}
$\frac{1}{10}$	$2.3879e^{-3}$	$1.6759e^{-3}$	$1.3760e^{-2}$	$9.8112e^{-3}$	3	$9.1474e^{-5}$	$6.5786e^{-5}$
$\frac{1}{20}$	$8.6047e^{-4}$	$6.0373e^{-4}$	$6.5907e^{-3}$	$4.7162e^{-3}$	7	$9.1472e^{-5}$	$6.5785e^{-5}$
$\frac{1}{40}$	$3.0834e^{-4}$	$2.1632e^{-4}$	$3.1163e^{-3}$	$2.2348e^{-3}$	9	$9.1494e^{-5}$	$6.5804e^{-5}$
$\frac{1}{80}$	$1.1004e^{-4}$	$7.7184e^{-5}$	$1.4634e^{-3}$	$1.0508e^{-3}$	11	$9.1483e^{-5}$	$6.5794e^{-5}$
$\frac{1}{160}$	$3.9131e^{-5}$	$2.7439e^{-5}$	$6.8491e^{-4}$	$4.9209e^{-4}$	15	$9.1484e^{-5}$	$6.5796e^{-5}$

Table 2 The results of L_∞ and L_{rms} for Example 4.1 by the presented spectral collocation method

$(\mathcal{S},\mathcal{T})$	Case I		Case II		Case III		Case IV	
	L_∞	L_{rms}	L_∞	L_{rms}	L_∞	L_{rms}	L_∞	L_{rms}
(2,2)	$6.3166e^{-2}$	$3.0132e^{-9}$	$6.7570e^{-2}$	$1.5474e^{-10}$	$4.9682e^{-2}$	$4.0990e^{-9}$	$4.7087e^{-2}$	$6.5717e^{-9}$
(4,4)	$7.1872e^{-9}$	$2.5344e^{-11}$	$2.9824e^{-9}$	$4.9920e^{-16}$	$2.9737e^{-9}$	$4.4848e^{-13}$	$2.9696e^{-9}$	$6.7123e^{-13}$
(6,6)	$5.7271e^{-13}$	$5.7460e^{-16}$	$4.0306e^{-13}$	$1.3012e^{-19}$	$4.0067e^{-13}$	$4.3882e^{-18}$	$4.0066e^{-13}$	$6.2867e^{-18}$
(8,8)	$2.9647e^{-20}$	$2.1906e^{-18}$	$1.2635e^{-19}$	$6.3486e^{-25}$	$1.2635e^{-19}$	$2.5908e^{-23}$	$1.2635e^{-19}$	$6.0413e^{-23}$
(10,10)	$2.7512e^{-25}$	$7.5460e^{-18}$	$1.8679e^{-25}$	$5.4818e^{-27}$	$1.8686e^{-25}$	$1.9316e^{-23}$	$1.8682e^{-25}$	$3.7296e^{-23}$

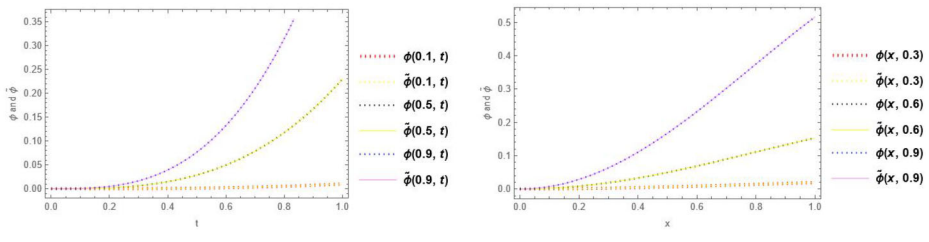

Figure 2 The plots in t-direction (left) and x-direction (right) for the numerical and actual solutions $\tilde{\phi}(x,t)$ and $\phi(x,t)$ for Example 4.1 in Case I with $\mathcal{S},\mathcal{T}=10$

Figure 2 represents the approximate solution $\phi(x,t)$ in x-direction as well as the t-direction of Example 4.1. Figure 3 shows the absolute error for Example 4.1 in xy-plane and in x- and t-directions, respectively. The convergence decay curve for this test Exam-

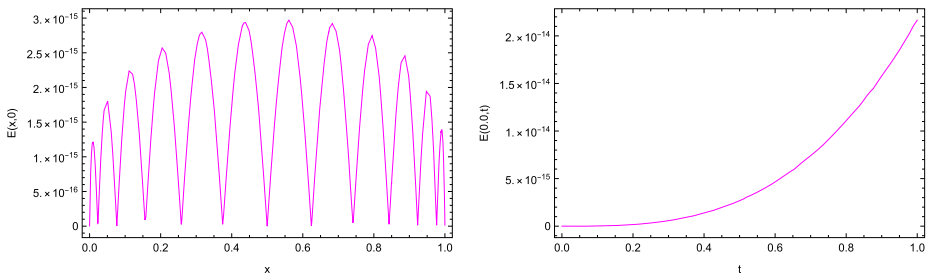

Figure 3 The plots in x-direction (left) and t-direction (right) for the numerical and actual solutions $\tilde{\phi}(x,t)$ and $\phi(x,t)$ for Example 4.1 in Case I with $\mathcal{S},\mathcal{T} = 10$

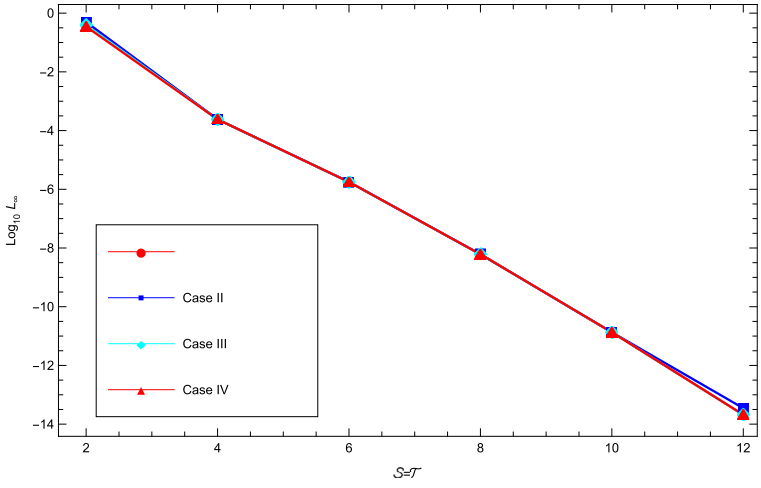

Figure 4 Convergence decay curve of Example 4.1

ple 4.1 is finally plotted for all Cases I-IV in Fig. 4. Obviously, by increasing the number of bases, our presented spectral algorithm produces more accurate outcomes.

Example 4.2 The second test problem is also devoted to 1D model equation (3.1)

$$ {}^{LC}\mathbb{D}_t^{\omega}\phi(x,t) + {}^{LC}\mathbb{D}_t^{\omega-1}\phi(x,t) + \phi(x,t) = \Delta\phi(x,t) + \mathcal{N}(x,t), \tag{4.4} $$

where we set $\zeta,\lambda = 1$, and the initial and boundary conditions and the right-hand side term $\mathcal{N}(x,t)$ are obtained from the exact solution $\phi(x,t) = x\cos\left(t^2 + x^2\right)$.

For the second test example, we set $\alpha = 0$, $\beta = 0$, and $\rho = 4$, $\sigma = -60$ for the bases parameters. We also take $\omega = 1.95$ and $\mathcal{S},\mathcal{T} = 10$. The approximated solution $\tilde{\phi}(x,t)$, along with the graph of absolute error $E(x,t)$ on the whole domain $[0,1]\times[0,1]$, is depicted in Fig. 5.

The numerical results for various values of $(\mathcal{S},\mathcal{T})$ and related to RMS error for these values of parameter and $\omega = 1.95$ are reported in Table 3. Besides, we also used diverse values $\omega = 1.25, 1.5$, and 1.75 in this table and presented the RMS errors. Similar outcomes with the same fractional orders but with the parameters $\alpha = 0$, $\beta = 0$, $\rho = 5$, $\sigma = -80$ are shown in Table 3. For comparison, the results of RMS errors achieved by the LMS [53] with the parameters $M = 201$, $m = 3$, and $N = 200$ and the radial basis functions (RBF) [54]

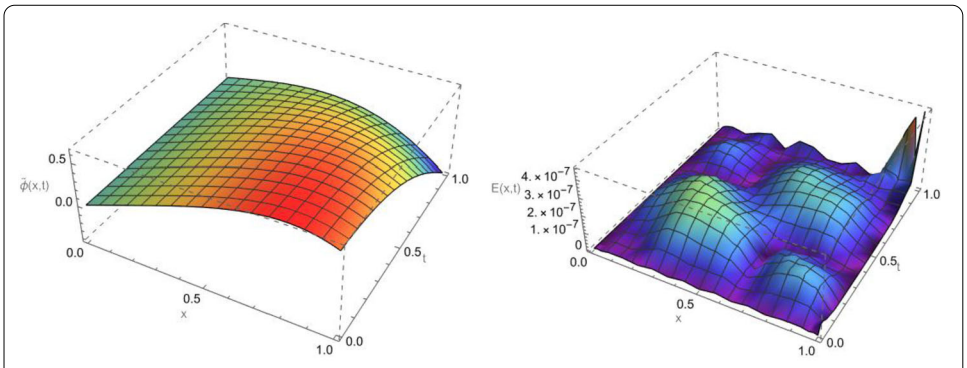

Figure 5 The approximate solution $\tilde{\phi}(x,t)$ (left) and the attained absolute errors (right) for Example 4.2, for $\alpha = 0, \beta = 0, \omega = 1.95, \rho = 4, \sigma = -60, \mathcal{S} = \mathcal{T} = 10$

Table 3 The results of L_{rms} for Example 4.2 by the presented spectral collocation method

$(\mathcal{S},\mathcal{T})$	$\alpha = 0, \beta = 0, \rho = 3, \sigma = -60$				$\alpha = 0, \beta = 0, \rho = 5, \sigma = -80$			
	$\omega = 1.25$	$\omega = 1.5$	$\omega = 1.75$	$\omega = 1.95$	$\omega = 1.25$	$\omega = 1.5$	$\omega = 1.75$	$\omega = 1.95$
(2,2)	$3.6388e^{-6}$	$2.0308e^{-6}$	$1.1590e^{-6}$	$7.7242e^{-7}$	$6.0294e^{-5}$	$2.7207e^{-6}$	$1.695e^{-6}$	1.6412–6
(4,4)	$3.9134e^{-4}$	$3.0107e^{-9}$	$3.0491e^{-9}$	$2.9368e^{-9}$	$4.1060e^{-9}$	$3.1874e^{-9}$	$2.4478e^{-11}$	$3.6371e^{-9}$
(6,6)	$8.6998e^{-12}$	$3.7272e^{-13}$	$1.7214e^{-13}$	$1.4195e^{-13}$	$8.1851e^{-12}$	$4.0499e^{-13}$	$2.9892e^{-13}$	$3.1396e^{-13}$
(8,8)	$1.1011e^{-13}$	$7.9274e^{-14}$	$1.0792e^{-13}$	$1.8100e^{-13}$	$4.3779e^{-13}$	$3.3217e^{-13}$	$2.5830e^{-13}$	$1.7112e^{-13}$
(10,10)	$5.8770e^{-17}$	$5.1179e^{-16}$	$4.6632e^{-16}$	$5.0703e^{-16}$	$1.9709e^{-16}$	$1.7492e^{-16}$	$1.4750e^{-16}$	$1.4387e^{-16}$

Table 4 The results of L_{rms} for Example 4.2 reported in [53] and [54]

M	δt	$\omega = 1.25$		$\omega = 1.5$		$\omega = 1.75$		$\omega = 1.95$	
		MLS [53]	RBF [54]	LMS [53]	RBF [54]	LMS [53]	RBF [54]	LMS [53]	RBF [54]
20	$\frac{1}{10}$	$2.2600e^{-4}$	$8.6205e^{-3}$	$1.1434e^{-3}$	$1.0377e^{-2}$	$4.6511e^{-3}$	$1.2172e^{-2}$	$1.1609e^{-2}$	$1.3240e^{-2}$
	$\frac{1}{30}$	$1.1860e^{-4}$	$3.7954e^{-3}$	$2.5318e^{-4}$	$5.3478e^{-3}$	$1.3350e^{-3}$	$6.4685e^{-3}$	$4.1575e^{-3}$	$5.3905e^{-3}$
	$\frac{1}{50}$	$1.1289e^{-4}$	$2.6038e^{-3}$	$1.4989e^{-4}$	$4.0987e^{-3}$	$7.6143e^{-4}$	$5.3163e^{-3}$	$2.5658e^{-3}$	$3.7930e^{-3}$
50	$\frac{1}{10}$	$1.8197e^{-4}$	$8.7725e^{-3}$	$1.1427e^{-3}$	$1.0560e^{-2}$	$4.6361e^{-3}$	$1.2388e^{-2}$	$1.1618e^{-2}$	$1.3476e^{-2}$
	$\frac{1}{30}$	$3.5426e^{-5}$	$3.8668e^{-3}$	$2.2873e^{-4}$	$5.4453e^{-3}$	$1.2702e^{-3}$	$6.5897e^{-3}$	$4.0390e^{-3}$	$5.5036e^{-3}$
	$\frac{1}{50}$	$2.2992e^{-5}$	$2.6551e^{-3}$	$1.0880e^{-4}$	$4.1743e^{-3}$	$6.8631e^{-4}$	$5.4164e^{-3}$	$2.4189e^{-3}$	$3.8800e^{-3}$

are tabulated in Table 4. It can be clearly seen that the results obtained by the presented spectral collocation approaches are superior to those obtained by the LMS and RBF.

Figure 6 represents the approximate solution $\phi(x,t)$ and x-direction of Example 4.2. Figure 7 shows the absolute error for Example 4.1 for xy-plane, t- and x-directions, respectively.

Example 4.3 Consider the one-dimensional time-fractional telegraph equation (3.1) given by

$$\begin{aligned} &{}^{LC}\mathbb{D}_t^{\omega}\phi(x,t) + \gamma_1\,{}^{LC}\mathbb{D}_t^{\omega-1}\phi(x,t) + \gamma_2\phi(x,t) \\ &\quad = e^{-x^2}\left(\frac{\gamma_1 t^{1-\omega}}{\Gamma(2-\omega)} + 2\gamma_3\left(-2tx^2 + t - 2x^3 + 3x\right) + \gamma_2(t+x)\right) + \gamma_3\Delta\phi(x,t), \end{aligned} \tag{4.5}$$

where $\zeta = \lambda = 1$. The associated initial and boundary conditions (3.2) are extracted from the exact true solution $\phi(x,t) = e^{-x^2}(t+x)$. To show the superiority of presented spectral

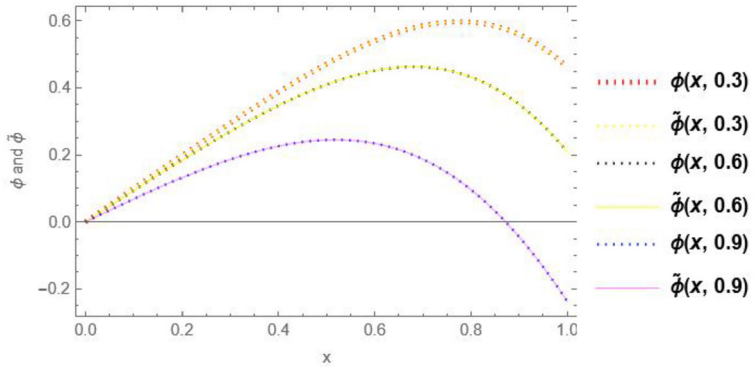

Figure 6 The plots of x-direction for the numerical and actual solutions $\tilde{\phi}(x,t)$ and $\phi(x,t)$ for Example 4.2, for $\alpha = 0$, $\beta = 0$, $\omega = 1.95$, $\rho = 4$, $\sigma = -60$, $\mathcal{S} = \mathcal{T} = 10$

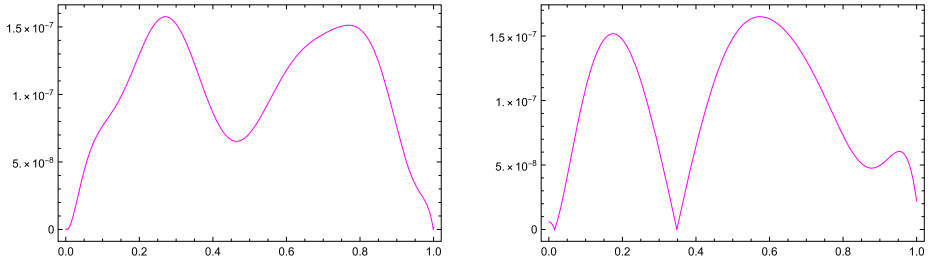

Figure 7 The plots in t-direction (left) and x-direction (right) for the absolute error $E(x,t)$ for Example 4.2 $\alpha = 0$, $\beta = 0$, $\omega = 1.95$, $\rho = 4$, $\sigma = -60$, $\mathcal{S} = \mathcal{T} = 10$

Table 5 The results of L_{rms} for Example 4.3 reported in [54] and the presented spectral collocation method

$\gamma_1, \gamma_2, \gamma_3$		$\omega = 1.05$	$\omega = 1.25$	$\omega = 1.5$	$\omega = 1.75$	$\omega = 1.95$
Finite difference scheme in [54] with $N = n = 50$						
$\gamma_1 = 0$	$\gamma_2 = \gamma_3 = 1$	$2.9337e^{-7}$	$3.5491e^{-7}$	$4.0820e^{-7}$	$4.5681e^{-7}$	$4.8627e^{-7}$
$\gamma_2 = 0$	$\gamma_1 = \gamma_3 = 1$	$1.7360e^{-3}$	$2.5572e^{-3}$	$4.0176e^{-3}$	$4.8585e^{-3}$	$1.9516e^{-3}$
$\gamma_3 = 0$	$\gamma_1 = \gamma_2 = 1$	$5.6870e^{-3}$	$9.1009e^{-3}$	$1.4579e^{-2}$	$1.6287e^{-2}$	$5.7435e^{-3}$
$\gamma_1 = 1$	$\gamma_2 = \gamma_3 = 0$	$7.5640e^{-3}$	$1.1838e^{-2}$	$1.7884e^{-2}$	$1.8785e^{-2}$	$6.3658e^{-3}$
$\gamma_2 = 1$	$\gamma_1 = \gamma_3 = 0$	$4.8373e^{-12}$	$9.3509e^{-12}$	$2.1439e^{-11}$	$5.2352e^{-11}$	$9.8006e^{-11}$
$\gamma_3 = 1$	$\gamma_1 = \gamma_2 = 0$	$3.1137e^{-7}$	$3.8019e^{-7}$	$4.3920e^{-7}$	$4.8890e^{-7}$	$5.1399e^{-7}$
Spectral collocation method with $\mathcal{S} = \mathcal{T} = 10$, $\rho = 3$, and $\sigma = -60$						
$\gamma_1 = 0$	$\gamma_2 = \gamma_3 = 1$	$5.78254e^{-18}$	$5.37119e^{-18}$	$5.09199e^{-18}$	$1.38906e^{-16}$	$2.20266e^{-16}$
$\gamma_2 = 0$	$\gamma_1 = \gamma_3 = 1$	$5.2451e^{-16}$	$4.8242e^{-16}$	4.0214^{-16}	$1.0215e^{-16}$	$1.8457e^{-16}$
$\gamma_3 = 0$	$\gamma_1 = \gamma_2 = 1$	5.38782^{-21}	$2.5391e^{-23}$	$1.49757e^{-23}$	$5.36477e^{-25}$	$3.81284e^{-25}$
$\gamma_1 = 1$	$\gamma_2 = \gamma_3 = 0$	$2.73434e^{-23}$	$2.12934e^{-23}$	$5.16168e^{-25}$	$6.05306e^{-25}$	$1.78471e^{-25}$
$\gamma_2 = 1$	$\gamma_1 = \gamma_3 = 0$	$4.63944e^{-34}$	$2.97414e^{-34}$	$6.51962e^{-35}$	$3.48841e^{-36}$	$3.53383e^{-11}$
$\gamma_3 = 1$	$\gamma_1 = \gamma_2 = 0$	$5.79337e^{-18}$	$5.37989e^{-18}$	$5.09908e^{-18}$	1.02856^{-16}	$1.6278e^{-16}$

collocation algorithm, we compare the achieved root mean square (RMS) error and absolute error in Table 5 for different values of γ_i, $i = 1, 2, 3$. The comparisons have been made between the results obtained using our technique and those obtained using the finite difference scheme [54]. It is evident that our results with less computational effort are more accurate in comparison with the finite difference scheme.

Example 4.4 As the first two-dimensional model problem, we take the following time-fractional telegraph equation (3.15)

$$ {}^{LC}\mathbb{D}_t^{\omega}\phi(x,y,t) + {}^{LC}\mathbb{D}_t^{\omega-1}\phi(x,y,t) + \phi(x,y,t) = t^4 + 24t^4\left(\frac{t^{-\omega}}{\Gamma(5-\omega)} + \frac{t^{1-\omega}}{\Gamma(6-\omega)}\right) + x^2 + y^2 - 4 + \Delta\phi(x,y,t). $$

Here, we set $\zeta_1 = \zeta_2 = \lambda = 1$, and the initial and boundary conditions are given from the actual true solution $\phi(x,t) = t^4 + x^2 + y^2$.

We first take $\alpha = 0$, $\beta = 0$, and $\rho = 4$, $\sigma = -40$ for this test problem. We also take $\omega = 1.95$ and $\mathcal{S}, \mathcal{V}, \mathcal{T} = 10$. The approximated solution $\tilde{\phi}(x,y,t=1)$, along with the graph of absolute error $E(x,y,t=0.5)$ on the whole domain $(x,y) \in [0,1] \times [0,1]$, is depicted in Fig. 8.

The results of RMS errors and maximum absolute values of errors for two different values of $\omega = 1.75, 1.95$ are shown in Table 6. These results are obtained by utilizing $\alpha = 0$, $\beta = 0$ and diverse values of (ρ, σ). To check the validity of the proposed spectral method, we compare the obtained results and the LMS outcomes [53] in Table 7.

Finally, for this test example, we represent the approximate solution $\phi(x,t)$ and x-direction. The results are presented in Fig. 9.

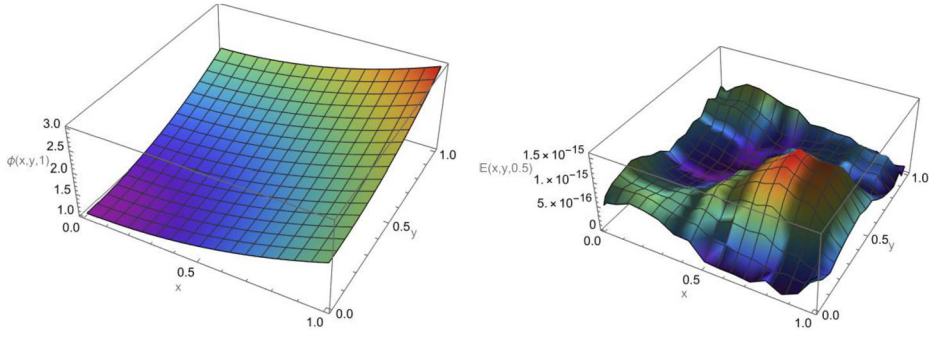

Figure 8 The approximate solution $\tilde{\phi}(x,y,1)$ (left) and the absolute error $E(x,y,0.5)$ (right) in Example 4.4, $\alpha = 0$, $\beta = 0$, $\omega = 1.95$, $\rho = 4$, $\sigma = -40$, $\mathcal{S} = \mathcal{T} = \mathcal{V} = 4$

Table 6 The results of L_∞ and L_{rms} for Example 4.4 by the presented spectral collocation method

	$\omega = 1.75, \alpha = \beta = 0$				$\omega = 1.95, \alpha = \beta = 0$			
(x,y,t)	(2,2,2)		(4,4,4)		(2,2,2)		(4,4,4)	
(ρ,σ)	L_∞	L_{rms}	L_∞	L_{rms}	L_∞	L_{rms}	L_∞	L_{rms}
(2,−20)	$5.9585e^{-2}$	$3.7755e^{-6}$	$2.6669e^{-34}$	$4.4109e^{-32}$	$5.5215e^{-2}$	$2.3922e^{-6}$	$6.5361e^{-35}$	$3.7737e^{-34}$
(3,−20)	$6.4172e^{-2}$	$4.2440e^{-7}$	$1.8760e^{-32}$	$1.2838e^{-34}$	$6.1069e^{-2}$	$4.8489e^{-7}$	$1.3235e^{-32}$	$8.718e^{-35}$
(4,−40)	$6.6603e^{-2}$	$3.4136e^{-9}$	$5.5338e^{-32}$	$3.5812e^{-36}$	$6.3587e^{-2}$	$4.0442e^{-7}$	$6.2967e^{-32}$	$2.6395e^{-36}$
(5,−65)	$6.9910e^{-2}$	$1.2574e^{-9}$	$1.3211e^{-27}$	$2.4234e^{-36}$	$6.8620e^{-2}$	$2.3597e^{-9}$	$1.3337e^{-27}$	$2.2957e^{-36}$
(10,−100)	$6.9012e^{-2}$	$2.1513e^{-9}$	$2.6866e^{-27}$	$2.7385e^{-36}$	$6.8240e^{-2}$	$3.5831e^{-9}$	$2.8261e^{-27}$	$3.4312e^{-36}$

Table 7 The results of L_∞ and L_{rms} for Example 4.4 reported in [53]

δt	$M = 2395, m = 5$			
	$\omega = 1.75$		$\omega = 1.95$	
	L_∞	L_{rms}	L_∞	L_{rms}
$\frac{1}{10}$	$2.8492e^{-2}$	$1.5193e^{-2}$	$6.2616e^{-2}$	$3.3332e^{-2}$
$\frac{1}{20}$	$1.2112e^{-2}$	$6.4347e^{-3}$	$3.0908e^{-2}$	$1.6419e^{-2}$
$\frac{1}{40}$	$5.0642e^{-3}$	$2.6646e^{-3}$	$1.5083e^{-2}$	$3.8419e^{-3}$
$\frac{1}{80}$	$2.0652e^{-3}$	$1.0621e^{-3}$	$3.5064e^{-3}$	$1.8240e^{-3}$
$\frac{1}{160}$	$7.9585e^{-4}$	$3.9004e^{-4}$	$1.6685e^{-3}$	$8.4691e^{-4}$

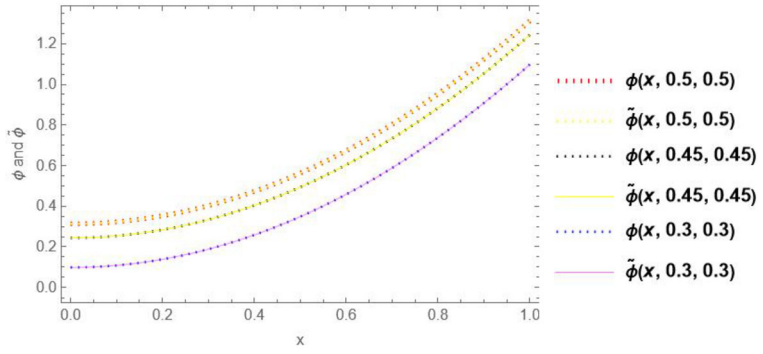

Figure 9 x-Direction for the approximate solution $\tilde{\phi}(x,t)$ and exact solution $\phi(x,t)$ in Example 4.4, for $\alpha = 0$, $\beta = 0$, $\omega = 1.95$, $\rho = 4$, $\sigma = -40$, $\mathcal{S} = \mathcal{T} = \mathcal{V} = 4$

Example 4.5 In the second test problem, we pay attention to the following time-fractional telegraph equation as a prototype of (3.15)

$$
\begin{aligned}
&{}^{LC}\mathbb{D}_t^{\omega}\,\phi(x,y,t) + {}^{LC}\mathbb{D}_t^{\omega-1}\phi(x,y,t) + \phi(x,y,t)\\
&\quad = t^4\left(\frac{24t^{1-\omega}}{\Gamma(6-\omega)} + \frac{24t^{-\omega}}{\Gamma(5-\omega)} + 2\pi^2 + 1\right)\sin(\pi(x+y)) + \Delta\phi(x,t).
\end{aligned}
$$

We set $\zeta_1 = \zeta_2 = \lambda = 1$. The exact true solution is given by $\phi(x,t) = t^4\sin(\pi(x+y))$. The corresponding initial and boundary conditions are extracted from the given actual solution.

Let us consider the next values of parameters $\alpha = 0$, $\beta = 0$, and $\rho = 2$, $\sigma = -65$ for this test problem. We also take $\omega = 1.7$ and $\mathcal{S}, \mathcal{V}, \mathcal{T} = 10$. The approximated solution $\tilde{\phi}(x,y,t=1)$, along with the graph of absolute error $E(x,y,t=0.5)$ on the whole domain $(x,y) \in [0,1] \times [0,1]$, is depicted in Fig. 10.

In Tables 8 and 9, we report the results of L_∞ and RMS errors between our technique and LMS [53] with 2025 uniform points and $m = 5$. Here, we used $\alpha = \beta = 0$, $\omega = 1.7, 1.9$, and $\rho = 2, 3$, $\sigma = -65$. Various equal values of $\mathcal{S} = \mathcal{V} = \mathcal{T} = 4, 6, 8, 10$ are also employed. It worth noting that the presented results are more accurate than the LMS results.

Figure 11 depicts the approximate solution $\phi(x,y,t)$ and x-direction of Example 4.5. Figures 12 and 13 visualize the absolute error for Example 4.5 for xy-plane, t-, x-, and y-directions, respectively.

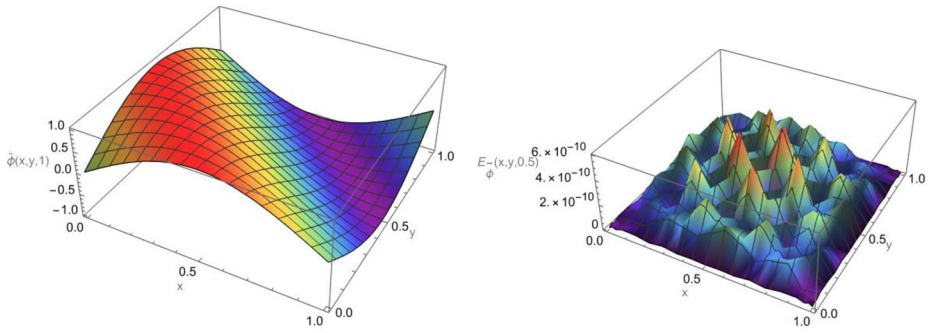

Figure 10 The approximate solution $\tilde{\phi}(x,y,t)$ (left) and the absolute errors (right) in Example 4.5, for $\alpha = 0$, $\beta = 0$, $\omega = 1.7$, $\rho = 2$, $\sigma = -65$, $\mathcal{S} = \mathcal{T} = \mathcal{V} = 10$

Table 8 The results of L_∞ and L_{rms} for Example 4.5 by the presented spectral collocation method

$\mathcal{S} = \mathcal{V} = \mathcal{T}$	$\omega = 1.7, \alpha = \beta = 0$				$\omega = 1.9, \alpha = \beta = 0$			
	$\rho = 2, \sigma = -65$		$\rho = 3, \sigma = -65$		$\rho = 2, \sigma = -65$		$\rho = 3, \sigma = -65$	
	L_∞	L_{rms}	L_∞	L_{rms}	L_∞	L_{rms}	L_∞	L_{rms}
4	$2.6571e^{-6}$	$4.6754e^{-16}$	$5.3714e^{-9}$	$8.5999e^{-16}$	$2.6113e^{-6}$	$3.0488e^{-16}$	$2.6560e^{-6}$	$5.8731e^{-16}$
6	$1.5063e^{-9}$	$3.0933e^{-18}$	$1.1223e^{-9}$	$4.7016e^{-18}$	$1.2842e^{-9}$	$2.9730e^{-18}$	$1.2059e^{-9}$	$4.4964e^{-18}$
8	$7.2278e^{-14}$	$6.1905e^{-21}$	$5.9399e^{-14}$	$8.7938e^{-21}$	$5.9647e^{-14}$	$6.0007e^{-21}$	$5.8763e^{-14}$	$8.4728e^{-21}$
10	$3.8742e^{-20}$	$2.1666e^{-25}$	$3.8549e^{-20}$	$1.3360e^{-25}$	$3.8781e^{-20}$	$4.2861e^{-25}$	$3.8572e^{-20}$	$1.3456e^{-25}$

Table 9 The results of L_∞ and L_{rms} for Example 4.4 reported in [53]

δt	$M = 2025, m = 5$ (uniform mesh)			
	$\omega = 1.7$		$\omega = 1.9$	
	L_∞	L_{rms}	L_∞	L_{rms}
$\frac{1}{5}$	$3.0420e^{-2}$	$1.5017e^{-2}$	$5.7458e^{-2}$	$2.8347e^{-2}$
$\frac{1}{10}$	$1.2917e^{-2}$	$6.3781e^{-3}$	$2.7619e^{-2}$	$1.3636e^{-2}$
$\frac{1}{20}$	$5.4532e^{-3}$	$2.6931e^{-3}$	$1.3079e^{-2}$	$6.4626e^{-3}$
$\frac{1}{40}$	$2.3351e^{-3}$	$1.1537e^{-3}$	$6.1953e^{-3}$	$3.0631e^{-3}$

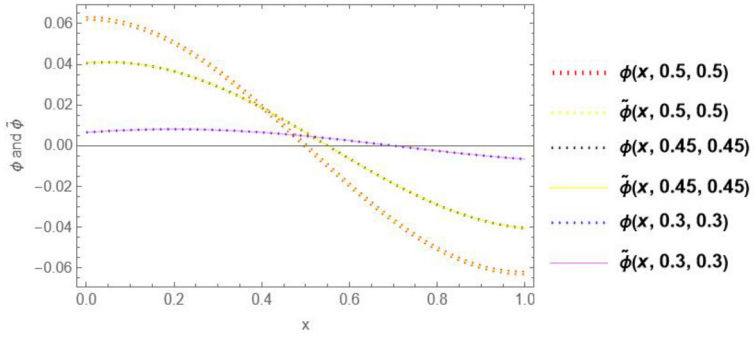

Figure 11 The plots of x-direction for the numerical and actual solutions $\tilde{\phi}(x,y,t)$ and $\phi(x,y,t)$ for Example 4.5, for $\alpha = 0$, $\beta = 0$, $\omega = 1.7$, $\rho = 2$, $\sigma = -65$, $\mathcal{S} = \mathcal{T} = \mathcal{V} = 10$

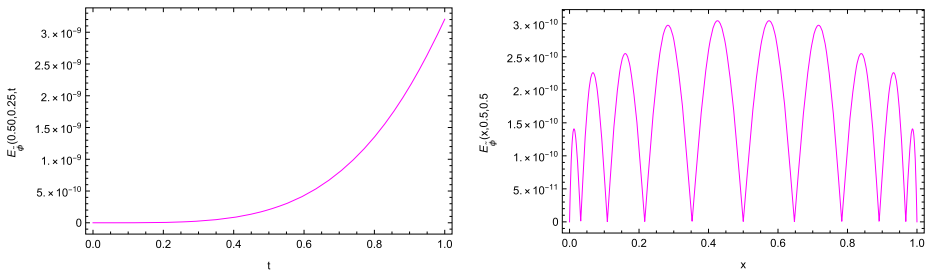

Figure 12 The plots of t-direction (left) and x-direction (right) for the attained absolute error $E(x,y,t)$ for Example 4.5 $\alpha = 0$, $\beta = 0$, $\omega = 1.7$, $\rho = 2$, $\sigma = -65$, $\mathcal{S} = \mathcal{T} = \mathcal{V} = 10$

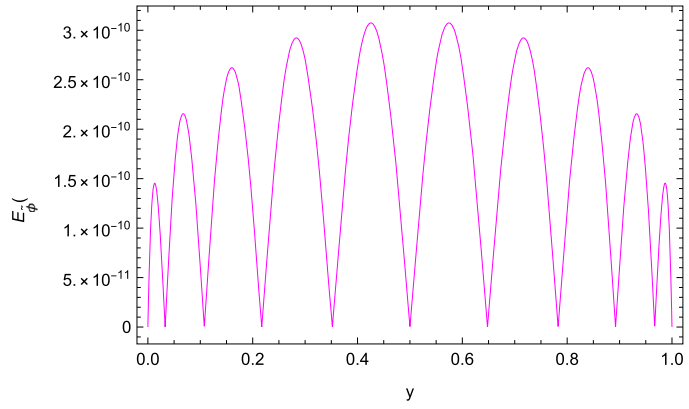

Figure 13 The plots of y-direction for the absolute error $E(x,y,t)$ in Example 4.5, for $\alpha = 0$, $\beta = 0$, $\omega = 1.7$, $\rho = 2$, $\sigma = -65$, $\mathcal{S} = \mathcal{T} = \mathcal{V} = 10$

5 Conclusion

In this work, we have presented a novel spectral algorithm for the efficient and accurate numerical solution of multi-dimensional telegraph equations of fractional order. The key strength of our approach lies in the use of Jacobi-Romanovski polynomials as the basis functions for the spectral technique, which possess several desirable properties, such as the ability to handle nonstandard domains and boundary conditions, as well as superior approximation capabilities. A comprehensive error analysis of the proposed model has been developed, providing valuable insights into the convergence rates and the factors that influence the accuracy of the numerical solutions. Some limitations of the proposed method can be noted, such as requiring higher computational resources when dealing with extremely irregular boundaries or highly complex geometries and reduced performance when applied to models involving very stiff differential equations or nonsmooth solutions. These challenges remain open issues that will be addressed in future work. In addition, through several numerical experiments, we have demonstrated the effectiveness of the proposed spectral algorithm in solving a range of multi-dimensional fractional-order telegraph equation models. The results showed that our method achieves significantly higher accuracy and computational efficiency compared to traditional numerical techniques. The algorithm proved to be a valuable asset in simulating complex models and achieving excellent results. Future work could focus on extending this approach to other important models, particularly those with irregular boundaries, as well as exploring adap-

tive techniques to optimize computational resources. This study paves the way for further exploration of fractional-order models in various fields, with promising applications in physics, engineering, and other scientific domains.

Acknowledgements
The authors would like to thank the anonymous reviewers and editor for providing helpful comments and suggestions which further improved the quality of the manuscript.

Author contributions
M.A. Abdelkawy: Conceptualization, Methodology, Investigation, Writing-Original draft preparation, Software, Visualization, Writing- Reviewing and Editing. Mohammad Izadi: Conceptualization, Methodology, Investigation, Writing-Original draft preparation, Visualization, Writing- Reviewing and Editing. Waleed Adel: Conceptualization, Methodology, Writing-Original draft preparation, Writing- Reviewing and Editing, Validation.

Funding
Not applicable.

Data availability
No datasets were generated or analysed during the current study.

Declarations

Ethics approval and consent to participate
Not applicable.

Consent for publication
Not applicable.

Competing interests
The authors declare no competing interests.

Author details
[1]Department of Mathematics and Statistics, College of Science, Imam Mohammad Ibn Saud Islamic University (IMSIU), Riyadh, Saudi Arabia. [2]Department of Mathematics, Faculty of Science, Beni-Suef University, Beni-Suef, Egypt. [3]Department of Applied Mathematics, Faculty of Mathematics and Computer, Shahid Bahonar University of Kerman, Kerman, Iran. [4]Laboratoire Interdisciplinaire de l'Universite' Francaise d'Egypte (UFEID Lab), Universite' Francaise d'Egypte, Cairo 11837, Egypt. [5]Department of Mathematics and Engineering Physics, Faculty of Engineering, Mansoura University, Mansoura 35516, Egypt.

Received: 25 June 2024 Accepted: 4 October 2024 Published online: 15 October 2024

References

1. Podlubny, I.: Fractional Differential Equations: An Introduction to Fractional Derivatives, Fractional Differential Equations, to Methods of Their Solution and Some of Their Applications. Elsevier, Amsterdam (1998)
2. Mainardi, F.: Fractional Calculus and Waves in Linear Viscoelasticity: An Introduction to Mathematical Models. World Scientific, Singapore (2022)
3. Podlubny, I.: Fractional-order systems and $PI^{\lambda}D^{\mu}$-controllers. IEEE Trans. Autom. Control **44**(1), 208–214 (1999)
4. Kilbas, A.A., Srivastava, H.M., Trujillo, J.J.: Theory and Applications of Fractional Differential Equations, vol. 204. Elsevier, San Diago (2006)
5. Caputo, M.: Linear models of dissipation whose *Q* is almost frequency independent-II. Geophys. J. Int. **13**(5), 529–539 (1967)
6. Caputo, M., Fabrizio, M.: A new definition of fractional derivative without singular kernel. Prog. Fract. Differ. Appl. **1**(2), 73–85 (2015)
7. Atangana, A., Baleanu, D.: New fractional derivatives with nonlocal and non-singular kernel: theory and application to heat transfer model. Therm. Sci. **20**(2), 763–769 (2016)
8. Evirgen, F.: Transmission of Nipah virus dynamics under Caputo fractional derivative. J. Comput. Appl. Math. **418**, Article ID 114654 (2023)
9. Bhangale, N., Kachhial, K.B., Gómez-Aguilar, J.F.: Fractional viscoelastic models with Caputo generalized fractional derivative. Math. Methods Appl. Sci. **46**(7), 7835–7846 (2023)
10. Li, X.Y., Liu, X.Y.: A hybrid kernel functions collocation approach for boundary value problems with Caputo fractional derivative. Appl. Math. Lett. **142**, Article ID 108636 (2023)
11. Suganya, S., Parthiban, V.: A mathematical review on Caputo fractional derivative models for COVID-19. AIP Conf. Proc. **2852**, Article ID 110003 (2023)
12. Dimitrov, Y., Georgiev, S., Todorov, V.: Approximation of Caputo fractional derivative and numerical solutions of fractional differential equations. Fractal Fract. **7**(10), Article ID 750 (2023)
13. Adel, W., Günerhan, H., Nisar, K.S., Agarwal, P., El-Mesady, A.: Designing a novel fractional order mathematical model for COVID-19 incorporating lockdown measures. Sci. Rep. **14**(1), 2926 (2024)
14. Srivastava, H.M., Adel, W., Izadi, M., El-Sayed, A.A.: Solving some physics problems involving fractional-order differential equations with the Morgan-Voyce polynomials. Fractal Fract. **7**(4), Article ID 301 (2023)

15. Tanenbaum, A.S., Wetherall, D.J.: Computer Networks, 5th edn. Pearson Education, Upper Saddle River (2011)
16. Haykin, S., Haykin, S.S.: Modern Wireless Communications. Pearson Education, Upper Saddle River (2005)
17. Okubo, A.: Application of the Telegraph Equation to Oceanic Diffusion, Another Mathematic Model, Chesapeake Bay Institute, the Johns Hopking Unversity Baltimore, MD, USA (1971)
18. Chang, C.-C., Werner, J.: A solution of the telegraph equation with application to two dimensional supersonic shear flow. J. Math. Phys. **31**(1–4), 91–101 (1952)
19. Kumar, Y., Srivastava, N., Singh, A., Singh, V.K.: Wavelets based computational algorithms for multidimensional distributed order fractional differential equations with nonlinear source term. Comput. Math. Appl. **132**, 73–103 (2023)
20. Kumar, Y., Singh, V.K.: Computational approach based on wavelets for financial mathematical model governed by distributed order fractional differential equation. Comput. Math. Simul. **190**, 1958–2017 (2020)
21. Kumar, Y., Yadav, P., Singh, V.K.: Distributed order Gauss-quadrature scheme for distributed order fractional sub-diffusion model. Chaos Solitons Fractals **170**, Article ID 113358 (2023)
22. Kumar, Y., Singh, S., Srivastava, N., Singh, A., Singh, V.K.: Wavelet approximation scheme for distributed order fractional differential equations. Comput. Math. Appl. **80**, 531–569 (2021)
23. Faheem, M., Khan, A.: A collocation method for time-fractional diffusion equation on a metric star graph with η edges. Math. Methods Appl. Sci. **46**(8), 8895–8914 (2022)
24. Faheem, M., Khan, A.: A wavelet collocation method based on Gegenbauer scaling function for solving fourth-order time-fractional integro-differential equations with a weakly singular kernel. Appl. Numer. Math. **184**, 197–218 (2023)
25. Faheem, M., Khan, A., Wong, P.J.Y.: A Legendre wavelet collocation method for 1D and 2D coupled time fractional nonlinear diffusion system. Comput. Math. Appl. **128**, 214–238 (2022)
26. Hussain, B., Faheem, M., Khan, A.: A numerical technique based on Legendre wavelet for linear and nonlinear hyperbolic telegraph equation. J. Appl. Math. Comput. **70**, 3661–3684 (2024)
27. Kumar, D., Deswal, K., Singh, S.: Wavelet-based approximation with nonstandard finite difference scheme for singularly perturbed partial integrodifferential equations. Comput. Appl. Math. **41**(8), Article ID 341 (2022)
28. Huang, F.: Analytical solution for the time-fractional telegraph equation. J. Appl. Math. **2009**, 890158 (2009)
29. Dhunde, R.R., Waghmare, G.L.: Double Laplace transform method for solving space and time fractional telegraph equations. Int. J. Math. Math. Sci. **2016**, Article ID 1414595 (2016)
30. Fino, A.Z., Ibrahim, H.: Analytical solution for a generalized space-time fractional telegraph equation. Math. Methods Appl. Sci. **36**(14), 1813–1824 (2013)
31. Mittal, R.C., Bhatia, R.: Numerical solution of second order one dimensional hyperbolic telegraph equation by cubic B-spline collocation method. Appl. Math. Comput. **220**, 496–506 (2013)
32. Nazir, T., Abbas, M., Yaseen, M.: Numerical solution of second-order hyperbolic telegraph equation via new cubic trigonometric B-splines approach. Cogent Math. **4**(1), Article ID 1382061 (2017)
33. Bansu, H., Kumar, S.: Numerical solution of space and time fractional telegraph equation: a meshless approach. Int. J. Nonlinear Sci. Numer. Simul. **20**(3–4), 325–337 (2019)
34. Asgari, M., Ezzati, R., Allahviranloo, T.: Numerical solution of time-fractional order telegraph equation by Bernstein polynomials operational matrices. Math. Probl. Eng. **2016**, Article ID 1683849 (2016)
35. Marasi, H.R., Derakhshan, M.H., Ghuraibawi, A.A., Kumar, K.: A novel method based on fractional order Gegenbauer wavelet operational matrix for the solutions of the multi-term time-fractional telegraph equation of distributed order. Math. Comput. Simul. **217**, 405–424 (2024)
36. Mulimani, M., Srinivasa, K.: Numerical solution of time-fractional telegraph equations using wavelet transform. Int. J. Dyn. Control **12**, 2166–2189 (2024)
37. Bai, X., Zhang, D., Shi, S., Yao, W., Guo, Z., Sun, J.: A fractional-order telegraph diffusion model for restoring texture images with multiplicative noise. Fractal Fract. **7**(1), Article ID 64 (2023)
38. Dubey, S., Chakraverty, S., Kundu, M.: Approximate solutions of space and time fractional telegraph equations using Taylor series expansion method. J. Comput. Anal. Appl. **31**(1), Article ID 48 (2023)
39. Izadi, M., Srivastava, H.M., Adel, W.: The nonlinear reactive transport model: an efficient approximation method based on quasilinearization and Bessel matrix method. Appl. Comput. Math. **23**(2), 135–158 (2024)
40. Abd-Elhameed, W.M., Al-Harbi, M.S., Amin, A.K., Ahmed, H.M.: Spectral treatment of high-order Emden-Fowler equations based on modified Chebyshev polynomials. Axioms **12**(2), Article ID 99 (2023)
41. Yadav, P., Jahan, S., Izadi, M.: Taylor wavelet quasilinearization method for solving tumor growth model of fractional order. Results Control Optim. **15**, Article ID 100437 (2024)
42. Izadi, M., Samei, M.E.: Time accurate solution to Benjamin-Bona-Mahony Burgers equation via Taylor-Boubaker series scheme. Bound. Value Probl. **2022**, Article ID 17 (2022)
43. Abdelkawy, M.A., Ahmed, E.A., Alqahtani, R.T.: Space-time spectral collocation algorithm for solving time-fractional Tricomi-type equations. Open Phys. **14**(1), 269–280 (2016)
44. Izadi, M., Srivastava, H.M.: The reaction-diffusion models in biomedicine: highly accurate calculations via a hybrid matrix collocation algorithm. Appl. Sci. **13**(21), Article ID 11672 (2023)
45. Andrews, G.E., Askey, R., Roy, R., Roy, R., Askey, R.: Special Functions, vol. 71. Cambridge University Press, Cambridge (1999)
46. Masjedjamei, M.: Three finite classes of hypergeometric orthogonal polynomials and their application in functions approximation. Integral Transforms Spec. Funct. **13**(2), 169–190 (2002)
47. Abo-Gabal, H., Zaky, M.A., Hafez, R.M., Doha, E.H.: On Romanovski-Jacobi polynomials and their related approximation results. Numer. Methods Partial Differ. Equ. **36**(6), 1982–2017 (2020)
48. Youssri, Y.H., Zaky, M.A., Hafez, R.M.: Romanovski-Jacobi spectral schemes for high-order differential equations. Appl. Numer. Math. **198**, 148–159 (2024)
49. Izadi, M., Veeresha, P., Adel, W.: The fractional-order marriage-divorce mathematical model: numerical investigations and dynamical analysis. Eur. Phys. J. Plus **139**(3), Article ID 205 (2024)
50. Rivlin, T.J.: An Introduction to the Approximation of Functions. Courier Corporation (1981)
51. Odibat, Z.M., Momani, S.: An algorithm for the numerical solution of differential equations of fractional order. J. Appl. Math. Inform. **26**(1), 15–27 (2008)

52. Delkhosh, M., Parand, K.: A hybrid numerical method to solve nonlinear parabolic partial differential equations of time-arbitrary order. Comput. Appl. Math. **38**(2), Article ID 76 (2009)
53. Kumar, A., Bhardwaj, A., Dubey, S.: A local meshless method to approximate the time-fractional telegraph equation. Eng. Comput. **37**, 3473–3488 (2021)
54. Hosseini, V.R., Chen, W., Avazzadeh, Z.: Numerical solution of fractional telegraph equation by using radial basis functions. Eng. Anal. Bound. Elem. **38**, 31–39 (2014)

Publisher's Note